The Plant Cell, Vol. 19: 131–147, January 2007, www.plantcell.org © 2007 American Society of Plant Biologists

Interactions among PIN-FORMED and P-Glycoprotein Auxin Transporters in *Arabidopsis* [W]

Joshua J. Blakeslee,[a,1,2] Anindita Bandyopadhyay,[a,1] Ok Ran Lee,[a,1,3] Jozef Mravec,[b] Boosaree Titapiwatanakun,[a] Michael Sauer,[b] Srinivas N. Makam,[a] Yan Cheng,[a] Rodolphe Bouchard,[c] Jiří Adamec,[d] Markus Geisler,[c] Akitomo Nagashima,[e] Tatsuya Sakai,[e] Enrico Martinoia,[c] Jiří Friml,[b] Wendy Ann Peer,[a,4] and Angus S. Murphy[a]

[a] Department of Horticulture, Purdue University, West Lafayette, Indiana 47907-2010
[b] Center for Plant Molecular Biology, University of Tübingen, D-72076 Tübingen, Germany
[c] Institute of Plant Biology, Basel–Zurich Plant Science Center, University of Zurich, CH-8007 Zurich, Switzerland
[d] Purdue Discovery Park, West Lafayette, Indiana 47907-2010
[e] Genetic Regulatory Systems Research Team, RIKEN Plant Science Center, Kanagawa, 230-0045, Japan

Directional transport of the phytohormone auxin is established primarily at the point of cellular efflux and is required for the establishment and maintenance of plant polarity. Studies in whole plants and heterologous systems indicate that PIN-FORMED (PIN) and P-glycoprotein (PGP) transport proteins mediate the cellular efflux of natural and synthetic auxins. However, aromatic anion transport resulting from PGP and PIN expression in nonplant systems was also found to lack the high level of substrate specificity seen in planta. Furthermore, previous reports that PGP19 stabilizes PIN1 on the plasma membrane suggested that PIN–PGP interactions might regulate polar auxin efflux. Here, we show that PGP1 and PGP19 colocalized with PIN1 in the shoot apex in *Arabidopsis thaliana* and with PIN1 and PIN2 in root tissues. Specific PGP–PIN interactions were seen in yeast two-hybrid and coimmunoprecipitation assays. PIN–PGP interactions appeared to enhance transport activity and, to a greater extent, substrate/inhibitor specificities when coexpressed in heterologous systems. By contrast, no interactions between PGPs and the AUXIN1 influx carrier were observed. Phenotypes of *pin* and *pgp* mutants suggest discrete functional roles in auxin transport, but *pin pgp* mutants exhibited phenotypes that are both additive and synergistic. These results suggest that PINs and PGPs characterize coordinated, independent auxin transport mechanisms but also function interactively in a tissue-specific manner.

INTRODUCTION

The principal natural auxin, indole-3-acetic acid (IAA), is a phytohormone that is polarly transported from sites of synthesis to distal sites of activity. IAA is an amphipathic weak acid that diffuses through cellular membranes only when protonated (IAAH) and is membrane-impermeant at neutral cytosolic pH (Goldsmith and Goldsmith, 1977; Blakeslee et al., 2005b; Li et al., 2005). Experimental evidence indicates that IAA is taken up into cells by a combination of lipophilic diffusion, proton-driven anionic (IAA^-) symport via AUXIN/LIKE-AUXIN (AUX/LAX) permeases (Bennett et al., 1996; Yang et al., 2006), and ATP-dependent uptake mediated by at least one inwardly directed P-glycoprotein (PGP) (Santelia et al., 2005; Terasaka et al., 2005). Cellular IAA^- export has been shown to be mediated by both the PIN-FORMED (PIN) efflux carrier proteins (Chen et al., 1998; Luschnig et al., 1998; Petrášek et al., 2006) and a subset of PGPs functioning as ATP-activated hydrophobic anion carriers (Geisler et al., 2005; Bouchard et al., 2006; Petrášek et al., 2006). Each of these proteins exhibits tissue-specific expression and subcellular localization patterns. In some tissues, the localization patterns of characterized PINs and PGPs overlap, and in other tissues, they do not (summarized in Supplemental Figure 1 online). For instance, PIN1 and PGP1 colocalize at shoot apices, and PIN2 coincides with PGP1 in epidermal cells proximal to the lateral root cap (Reinhardt et al., 2003; Geisler et al., 2005; Heisler et al., 2005). However, it is not clear whether colocalizing PINs and PGPs interact to affect the direction, velocity, or specificity of transported substrates.

PINs are members of the unique auxin efflux carrier (TC 2.A.69) protein family with predicted membrane topology similar to ion-coupled members of the major facilitator (TC 2.A.1) transport protein family (Müller et al., 1998). The *PIN* family in *Arabidopsis thaliana* consists of eight expressed members. Mutations in *pin* genes result in phenotypes consistent with altered auxin transport ranging from pin-formed inflorescences in *pin1* to agravitropic roots in *pin2* (Chen et al., 1998; Gälweiler et al., 1998; Luschnig et al., 1998). However, some *pin* mutants, such as *pin4*, exhibit no obvious phenotypes (Friml et al., 2002a).

PIN proteins have been shown to independently activate auxin transport in both plant and heterologous cell expression systems (Chen et al., 1998; Luschnig et al., 1998; Petrášek et al., 2006).

[1] These authors contributed equally to this work.
[2] Current address: Department of Biology, Brown University, Providence, RI 02912.
[3] Current address: Department of Biology, Chungnam National University, Daejeon 305-764, Korea.
[4] To whom correspondence should be addressed. E-mail peerw@purdue.edu; fax 765-494-0391.
The author responsible for distribution of materials integral to the findings presented in this article in accordance with the policy described in the Instructions for Authors (www.plantcell.org) is: Angus S. Murphy (murphy@purdue.edu).
[W] Online version contains Web-only data.
www.plantcell.org/cgi/doi/10.1105/tpc.106.040782

However, it is still not clear whether the substrate specificity of auxin transport in whole plants and protoplasts (Geisler et al., 2005; Bouchard et al., 2006) can be attributed to PIN proteins alone. In heterologous expression systems, PIN expression activated the efflux of IAA and the artificial auxin 1-naphthyleneacetic acid, but it also activated the efflux of benzoic acid (BA), a weak acid that is not polarly transported in planta (Petrášek et al., 2006). Furthermore, auxin efflux activity in untransformed BY-2 cells with no detectable background *PIN* expression was substantially sensitive to the auxin efflux inhibitor naphthylthalamic acid (see Figure 2B in Petrášek et al., 2006), which may be attributable in part to endogenous PGP activity.

PIN-mediated auxin efflux appears to be sufficient to establish and maintain the polarity of plant development, as the profound defects in organismal polarity found in double and triple *pin* mutants (Benkova et al., 2003; Blilou et al., 2005) have not been seen in *pgp* or *aux1/lax* mutants to date. Mutational, developmental, and cell biological evidence unequivocally demonstrates that PINs are responsible for determining the vector of auxin transport (Weijers et al., 2005; Wisniewska et al., 2006).

PGPs are plant homologs of the integral membrane ATP binding cassette (TC 3.A.1) phosphoglycoproteins (ABCB/MDR/PGP) that mediate the efflux of chemotherapeutics from human cells. PGPs share a common mechanism whereby they bind membrane-embedded amphipathic substrates and move them to the surface of the opposing membrane leaflet in an ATP-dependent manner (Ambudkar et al., 2005; Blakeslee et al., 2005b; Callaghan et al., 2006; Dawson and Locher, 2006; Yin et al., 2006). Compared with humans, in which six PGP isoforms are found, the plant PGP subfamily is expanded (21 expressed members in *Arabidopsis* and 17 in rice [*Oryza sativa*]) and exhibits more sequence diversity (Martinoia et al., 2002; Geisler and Murphy, 2006). Some PGPs are not apparently involved in auxin transport. Cj MDR1 from the medicinal plant *Coptis japonica*, which exhibits domain-specific divergence from auxin-transporting PGPs, exhibits specificity for alkaloids such as berberine (Yazaki et al., 2001). However, no plant PGP identified to date exhibits the type of broad-substrate specificity associated with the mammalian PGP1.

Mutations in *Arabidopsis*, maize (*Zea mays*), and sorghum (*Sorghum bicolor*) *PGP* genes result in reduced long-distance auxin transport, reduced auxin loading in apical tissues, and hypomorphic/hypertropic growth phenotypes consistent with altered auxin movement (Noh et al., 2001; Geisler et al., 2003, 2005; Multani et al., 2003; Lin and Wang, 2005; Santelia et al., 2005; Terasaka et al., 2005). However, *pgp* double mutants exhibit only minor alterations in organ polarity, suggesting that PGPs are not required for the basal levels of auxin movement required for normal early development. ATPGP1, PGP19/ATMDR1, and PGP4 (hereafter referred to as PGP1, PGP19, and PGP4, respectively) have been shown to mediate the energy-dependent movement of auxins and, to a lesser extent, other aromatic carboxylate compounds, but not that of common hydrophobic substrates of mammalian PGPs (Noh et al., 2001, 2003; Geisler et al., 2003, 2005; Terasaka et al., 2005; Bouchard et al., 2006). The apparent mechanism of PGP-mediated auxin efflux is consistent with a role in excluding auxin reuptake from the plasma membrane (Blakeslee et al., 2005b).

Previous reports suggested that PGPs regulate the plasma membrane stability of PIN proteins and that there might be specific PIN–PGP protein interactions (Noh et al., 2003). In *Arabidopsis*, PIN1 was found to be delocalized in xylem parenchyma cells of hypertropic *pgp19* hypocotyls, but not in *pgp1* hypocotyls that exhibited relatively normal rates of tropic bending. These results suggest a more direct interaction between PIN1 and PGP19 than between PIN1 and PGP1. A precedent for a synergistic interaction is found in yeast, in which a genetic interaction between the ABC pleiotropic drug resistance protein transporter PDR5p and the hexose major facilitator protein transporters HXT11 and HXT9 has been demonstrated (Nourani et al., 1997).

We focused our attention on the best characterized PINs (PIN1 and PIN2) and PGPs (PGP1, PGP4, and PGP19) and examined their spatial, biochemical, and functional relationships in planta and in heterologous expression systems. Here, we present an analysis of combined *pin* and *pgp* mutant phenotypes and PIN/PGP colocalization in planta. We also analyze direct and functional PIN–PGP interactions in vitro and in heterologous systems. We show that PIN–PGP interactions can enhance substrate specificity and activate (or antagonize) the direction of cellular auxin transport across the plasma membrane. Finally, for contrast, we analyze PIN and PGP interactions with the AUX1 auxin permease (TC 2.A.18) and, consistent with *aux1* growth phenotypes (Bennett et al., 1996; Marchant et al., 1999), find no evidence of direct interactions of either protein with AUX1.

RESULTS

PGP19 mRNA and Protein Localization

The tissue-specific distribution patterns of *PGP19* have not previously been described in detail; this information is important for understanding where PGP19 functions in the plant. In situ hybridization analysis showed that *PGP19* was strongly expressed throughout the cotyledonary node and throughout the upper hypocotyl of light-grown seedlings (Figures 1A to 1D, 1G, and 1H). *PGP19* expression was increasingly restricted to the vascular tissue in hypocotyl regions distal to the node (Figure 1E). By contrast, *PGP19* expression in dark-grown seedlings was observed throughout the hypocotyl (Figure 1F). *PGP19* was also strongly expressed throughout the root (Figures 1I and 1J). This finding is consistent with previously published β-glucuronidase (GUS) expression analysis (Noh et al., 2001). *PGP19* expression increased by 5-fold in dark-grown wild-type and *pgp1* seedlings, whereas *PGP1* expression increased by 14- and 8-fold in dark-grown wild-type and *pgp19* seedlings, respectively. In real-time quantitative PCR analysis of upper inflorescence stems, *PGP19* expression was enriched by approximately twofold in the inner tissues compared with the outer tissues, whereas *PGP1* was equally expressed, consistent with microarray data (Suh et al., 2005).

A PGP19-specific antiserum was prepared to a peptide derived from the soluble loop region of the protein (see Methods). Neither the preimmune serum in the wild type nor the PGP19 antiserum in *pgp19* hypocotyls or roots had a signal (Figures 1O, 1P, 1U, and 1V). Using this PGP19 antiserum in the wild type,

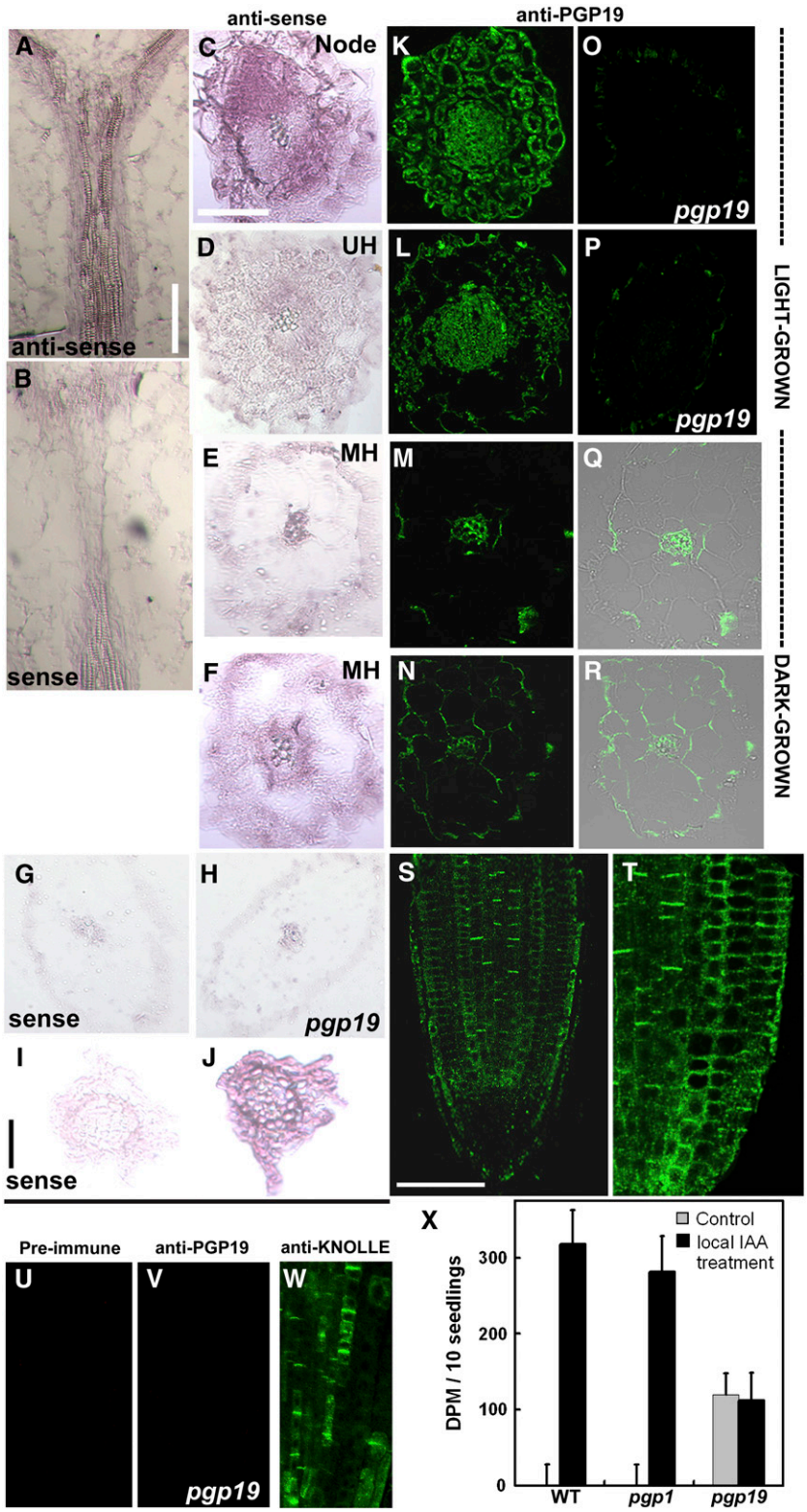

Figure 1. PGP19 Localization in Light- and Dark-Grown Seedlings.

(A) to **(J)** Localization of *PGP19* expression using in situ hybridization in 7-d-old seedlings. All seedlings are wild type (Wassilewskija [Ws]) unless indicated otherwise. Bars = 50 μm.

PGP19 localization coincided with *PGP19* expression in the hypocotyls of light- and dark-grown seedlings (Figures 1K to 1N, 1Q, and 1R). In whole mount roots, a PGP19 signal at the plasma membrane was more abundant on the lower end of cells in the epidermis, cortex, and stele (Figures 1S and 1T); this signal was stably associated with the formation of lower cell walls (Figures 1S and 1T). However, the PGP19 signal was not associated with early cell plate formation, as seen with the cytokinesis marker KNOLLE (Figure 1W), indicating that PGP19 is not associated with early cell plate formation. Apolar PGP19 signals were observed in the pericycle, endodermis, and newly divided provascular cells of roots (Figures 1S and 1T).

PGP19 Functions in Long-Distance Auxin Transport and Auxin Retention in the Stele

Detailed analysis of auxin movement and mutant phenotypes indicates that PIN1 mediates the vectorial movement of auxin from the shoot apex to the root apex as well as localized auxin flow required for embryogenesis and aerial organ development (Tanaka et al., 2006). Consistent with localization in apical tissues (Figures 1G, 1K, 1S, and 1T), PGP19 appears to function coordinately with PGP1 in loading of auxin into basipetal streams at the shoot and root tip (Blakeslee et al., 2005b). However, PGP19 also plays an additional role in long-distance auxin transport, as shoot basipetal IAA transport is reduced by >50% in *pgp19* (Noh et al., 2001) compared with a reduction of 27 ± 12% in *pin1-7* using the same methods. This finding is consistent with PGP19 localization in the vascular bundle and immediately adjacent cells (Figures 1M, 1S, and 1T).

The localization of PGP19 in the root endodermis and pericycle suggests that PGP19 may enhance long-distance transport by preventing auxin entry into the plasmalemma of the cell layer adjacent to the primary vascular transport stream. We designed an experiment to measure the escape of auxin from the polar vascular stream by collection and counting of discontinuous cellulose/silica gel media strips supporting the mature portion of the seedling root (see Methods). Enhanced [^{3}H]IAA efflux out of the stele was observed in *pgp19* roots but not in wild type or *pgp1* roots ($P < 0.001$; Figure 1X). A prediction from this model would be that increasing the auxin flux through the vascular stream would overwhelm the PGP19-mediated barrier effect and result in enhanced auxin export into the nonstelar apoplast. Consistent with that prediction, increasing the auxin flux by the addition of an extra 100 pmol of cold IAA resulted in increased stelar [^{3}H]IAA efflux in the wild type and *pgp1* but not in *pgp19*

Figure 1. (continued).

(A), **(C)** to **(F)**, **(H)**, and **(J)** Antisense probe.
(B), **(G)**, and **(I)** Sense probe.
(A) to **(E)** and **(G)** to **(J)** Light-grown seedlings.
(F) Dark-grown seedling.
(A) Cotyledonary node and upper hypocotyl longitudinal section with an antisense probe shows signal in the vascular bundle.
(B) Cotyledonary node and upper hypocotyl longitudinal section with a sense probe shows no signal.
(C) Cotyledonary node cross section shows strong signal throughout the node.
(D) Upper hypocotyl (UH; below the cotyledonary node) cross section shows signal throughout the hypocotyl.
(E) Mid hypocotyl (MH) cross section shows signal restricted to the vascular bundle.
(F) Mid hypocotyl cross section of a dark-grown seedling shows signal throughout the hypocotyl.
(G) Hypocotyl cross section with a sense probe shows no signal.
(H) Hypocotyl cross section of a light-grown *pgp19* seedling with an antisense probe shows no signal.
(I) Root cross section with a sense probe shows no signal.
(J) Root cross section with an antisense probe shows strong signal throughout the root.
(K) to **(U)** Immunohistochemical localization of PGP19 using PGP19-specific antiserum, unless indicated otherwise. All are 7-d-old wild-type (Ws) seedlings unless indicated otherwise. Bars = 50 μm.
(K) to **(Q)** and **(S)** to **(W)** Light-grown seedlings.
(N) and **(R)** Dark-grown seedlings.
(K) Cotyledonary node cross section shows strong signal throughout tissue.
(L) Upper hypocotyl (below the cotyledonary node) cross section shows signal throughout tissue.
(M) Mid hypocotyl cross section shows signal in the vascular bundle.
(N) Mid hypocotyl cross section of a dark-grown seedling shows signal throughout tissue.
(O) Cotyledonary node cross section of a *pgp19* seedling does not show signal.
(P) Hypocotyl cross section of a *pgp19* seedling does not show signal.
(Q) Bright-field overlay of **(M)**.
(R) Bright-field overlay of **(N)**.
(S) Whole mount root tip of a 5-d-old light-grown seedling shows signal in the stele, endodermis, pericycle, and cortex.
(T) Detail of the root tip shown in **(S)**.
(U) Preimmune serum in whole mount root tip of a 5-d-old seedling does not show signal.
(V) Whole mount root tip of a 5-d-old *pgp19* seedling does not show signal.
(W) KNOLLE, using anti-KNOLLE (green), signal localizes at the cell plate during cytokinesis in a 5-d-old seedling.
(X) Movement of [^{3}H]IAA from stelar flow into the cortical/epidermal apoplast of mature root tissues before (gray bars) and after (black bars) application of additional cold IAA to the root–shoot transition zone. [^{3}H]IAA was initially applied to the shoot apex in a discontinuous system to establish polar flow. Data are means ± SD ($n = 10$).

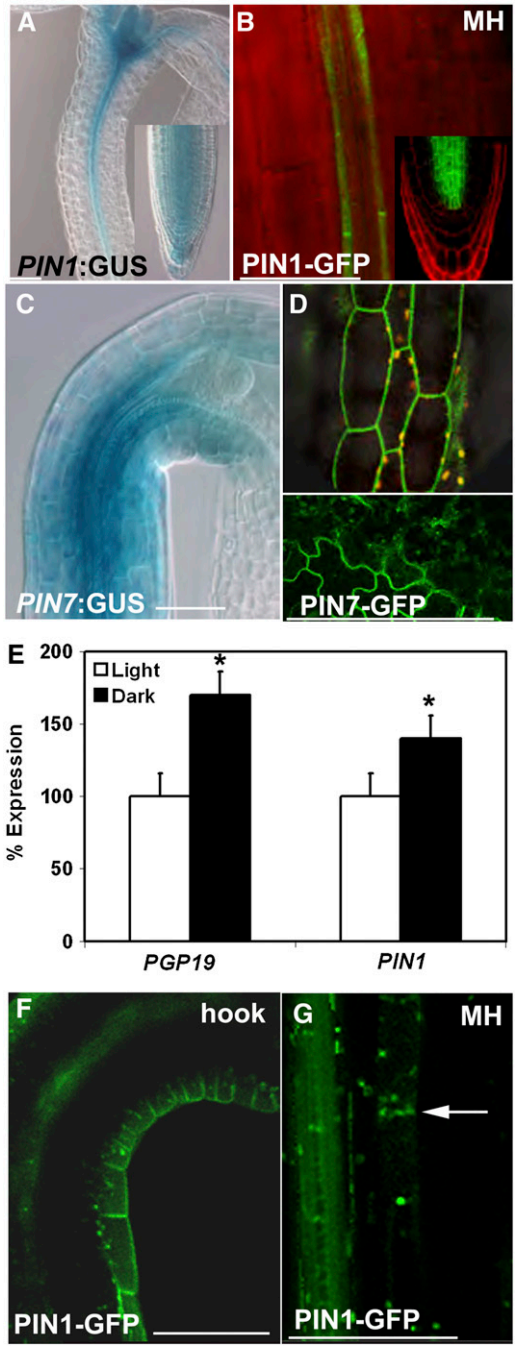

Figure 2. PIN1 Localization in Light- and Dark-Grown Seedlings.

(A) Pro$_{PIN1}$:GUS activity is observed at the shoot apex, in vascular tissue, and in the root tip of a light-grown seedling.

(B) Pro$_{PIN1}$:PIN1-GFP fluorescence is observed in the xylem parenchyma in hypocotyl and root tip in a light-grown seedling. MH, mid hypocotyl.

(C) Pro$_{PIN7}$:PIN7-GUS activity is observed at the node and throughout the hypocotyl in a dark-grown seedling. The abundance of PIN7 in leaf cells may contribute to the substrate specificity seen in protoplast transport assays (Geisler et al., 2005).

(D) Pro$_{PIN7}$:PIN7-GFP fluorescence is apolar in the epidermis of hypocotyls (top) and cotyledons (bottom).

(Figure 1X). This result is consistent with an increased lateral movement of auxin, presumed to be a factor in the hypergravitropic bending observed in *pgp19* mutants (Noh et al., 2003).

PIN1 mRNA and Protein Localization in *Arabidopsis* Hypocotyls

PIN1 is abundant in inflorescence apices (Reinhardt et al., 2003; Heisler et al., 2005), and *PIN1* expression becomes restricted to vascular tissues below the apex with >10-fold enrichment in the inner tissues of upper inflorescences in real-time quantitative PCR analysis, consistent with previous data (Gälweiler et al., 1998; Suh et al., 2005). By contrast, *PIN7* expression was enriched by ~1.2-fold in inner tissues of upper inflorescences in real-time quantitative PCR, consistent with microarray analysis (Suh et al., 2005). In light-grown hypocotyls, *PIN1* expression, visualized with a Pro$_{PIN1}$:PIN1-GUS reporter, was strong at the apex and in the vascular tissue (Figure 2A), and Pro$_{PIN1}$:PIN1–green fluorescent protein (GFP) signals were restricted to the vascular tissue below the cotyledonary node (Figure 2B). This suggests that a PIN1 immunolocalization signal previously observed in cortical and bundle sheath cells of light-grown hypocotyls (Noh et al., 2003) was nonspecific. It is also somewhat unlikely that signals observed outside the vascular strand in light-grown hypocotyls were the result of the PIN1 antiserum cross-reacting with PIN7, because, although *PIN7* is expressed in these tissues (Figure 2C), Pro$_{PIN7}$:PIN7-GFP exhibits an apolar localization in these tissues (Figure 2D).

As was seen with *PGP19*, *PIN1* expression increased in dark-grown seedlings ($P < 0.05$; Figure 2E). In dark-grown seedlings, PIN1 signal was observed in the vascular parenchyma and epidermis of the shoot apical hook (Figure 2F) and in the vascular parenchyma and the adjacent cortical cells in the mid hypocotyl (Figure 2G), consistent with previous reports (Blakeslee et al., 2004). Therefore, direct subcellular interactions of PIN1 and PGP19 are likely only at the shoot and root apices and in bundle sheath cells of dark-grown hypocotyls.

Colocalization: Overlapping Patterns of Expression and Localization

The expression patterns of *PGP1*, *PGP19*, *PIN1*, and *PIN2* in roots from the AREX database (www.arexdb.org; Birnbaum et al., 2003) are presented in Figure 3A. *PIN1* and *PGP19* expression patterns appeared to overlap strongly in the stele and endodermis. In the cotyledonary node and upper hypocotyl, *PIN1* and *PGP19* expression overlapped in vascular and bundle

(E) Expression of *PGP19* and *PIN1* in 5-d-old light- and dark-grown seedlings. The light-grown value was set to 100% for each gene. Data are means ± SD ($n = 3$). * $P < 0.05$.

(F) Pro$_{PIN1}$:PIN1-GFP fluorescence is observed in the xylem parenchyma and epidermis in the apical hook of a dark-grown seedling.

(G) Pro$_{PIN1}$:PIN1-GFP fluorescence is observed in the xylem parenchyma and adjacent cortical cell (arrow) in the hypocotyl of a dark-grown seedling.

Bars = 100 μm.

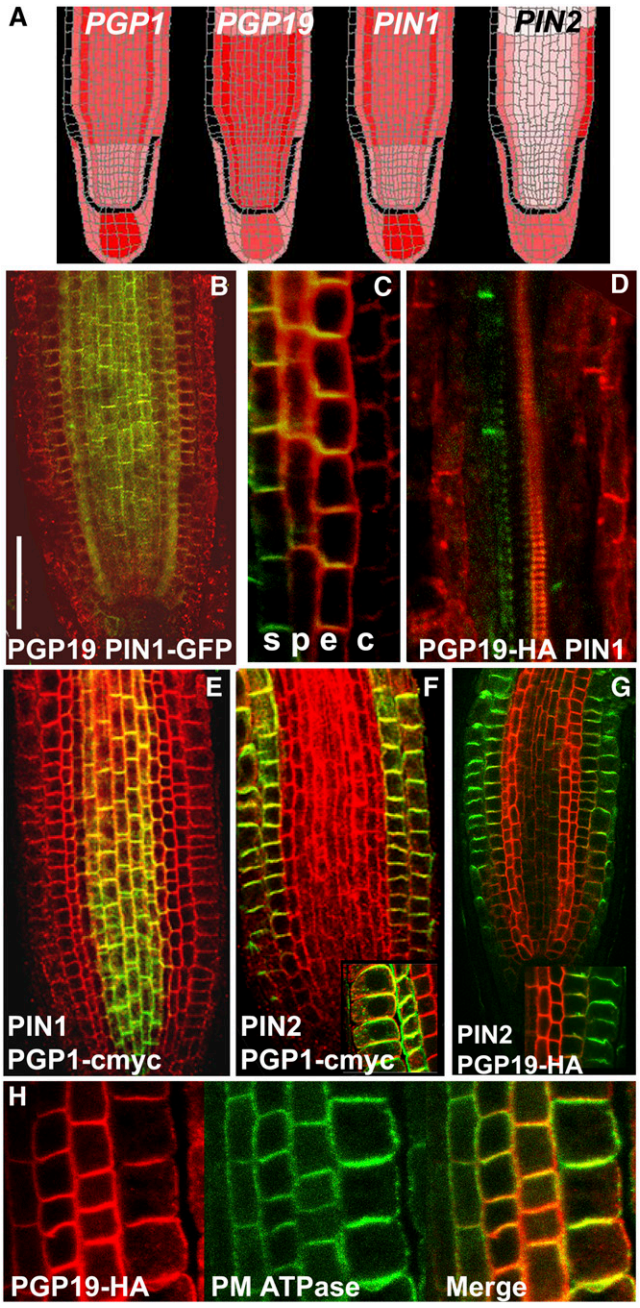

Figure 3. Overlapping Patterns of Expression and Localization.

(A) Heat map of root tips from the AREX database (www.arexdb.org) showing the expression of *PGP1*, *PGP19*, *PIN1*, and *PIN2*. Relative expression is proportional to color intensity.

(B) to **(H)** PGP localizations are shown in red; PIN and ATPase localizations are shown in green; colocalization is shown in yellow. All images show coimmunolocalizations in 5-d-old light-grown seedlings. Bar = 50 μm.

(B) PGP19 and Pro$_{PIN1}$:PIN1-GFP in the root.

(C) Pro$_{PGP19}$:PGP19-HA and PIN1 in the root. s, stele; p, pericycle; e, endodermis; c, cortex. Pro$_{PGP19}$:PGP19-HA complements the phenotype of *pgp19*. The PGP19-HA construct was used previously by Petrášek et al. (2006).

(D) Pro$_{PGP19}$:PGP19-HA and PIN1 in the hypocotyl.

(E) Pro$_{PGP1}$:PGP1-cmyc and PIN1 in the root.

(F) Pro$_{PGP1}$:PGP1-cmyc and PIN2 in the root.

(G) Pro$_{PGP19}$:PGP19-HA and PIN2 in the root.

(H) Pro$_{PGP19}$:PGP19-HA and plasma membrane (PM) ATPase in the root.

sheath tissues in light- and dark-grown seedlings (Figures 1A, 1C, 2A, and 2F).

PGP19, PIN1, and PIN2 were coimmunolocalized in roots and hypocotyls. PGP19 and Pro$_{PIN1}$:PIN1-GFP signals overlapped in the stele, endodermis, and pericycle of roots (Figure 3B). Pro$_{PGP19}$:PGP19-hemagglutin (HA) and PIN1 signals were similar to those with the native PGP19 antibody and Pro$_{PIN1}$:PIN1-GFP, although the signal in the stele was reduced; a detail of the coimmunolocalization in roots is shown in Figure 3C. Pro$_{PGP19}$:PGP19-HA and PIN2 signals overlapped in cortical cells in the root (Figure 3G). As a control, Pro$_{PGP19}$:PGP19-HA was coimmunolocalized with plasma membrane H^+-ATPase (AHA), and the signals overlapped in the root epidermal, cortical, and endodermal cells (Figure 3H).

Although *PIN1* and *PGP19* expression overlap at the node and vascular tissue in hypocotyls, in the mid hypocotyl of light-grown seedlings, polar PGP19 signals in bundle sheath and cortical cells did not overlap with Pro$_{PIN1}$:PIN1-GFP signals that were restricted to vascular parenchyma cells (Figure 3D). In addition to polar localization, a weaker PGP19 localization was observed on lateral membranes in cortical cells in hypocotyls (Figure 3D), where PIN3 was previously localized (Friml et al., 2002b). This finding suggests possible interactions with PIN3-mediated redirection of auxin from bundle sheath to vascular transport streams; those interactions are currently being pursued in the context of phototropic bending.

PGP1, PIN1, and PIN2 were also coimmunolocalized in roots. Pro$_{PGP1}$:PGP1-cmyc signal overlapped with PIN1 in stelar tissues between the lateral root cap and the distal elongation zone of the root (Figure 3E) and with PIN2 signal in cortical and epidermal cells in the same region (Figure 3F). This suggests that possible PGP1–PIN interactions in this region could mediate the delivery of redirected auxin accumulated in the lateral root cap by AUX1 and PGP4 to the elongation zone. Consistent with this function, auxin transport from the root apex has been shown to be reduced in this region in *pgp1* mutants (Geisler et al., 2005).

Genetic Analysis Suggests Both Additive and Synergistic Auxin Transport Mechanisms

Crosses of *pgp* with *pin* mutants were made to determine whether there was a genetic interaction affecting shoot phenotypes. The phenotypes of the wild type and the single mutants are presented in Figures 4A to 4C. The wild-type plants had extended inflorescence stems as well as axillary and secondary inflorescences, rosette and cauline leaves were present and numerous, and flowers and siliques were present (Figure 4A). *pgp1 pgp19* plants were dwarfed with short inflorescences, reduced axillary and secondary inflorescences, and reduced numbers of rosette and cauline leaves, which were smaller and curled; flowers and siliques were present (Figure 4B). *pin1*

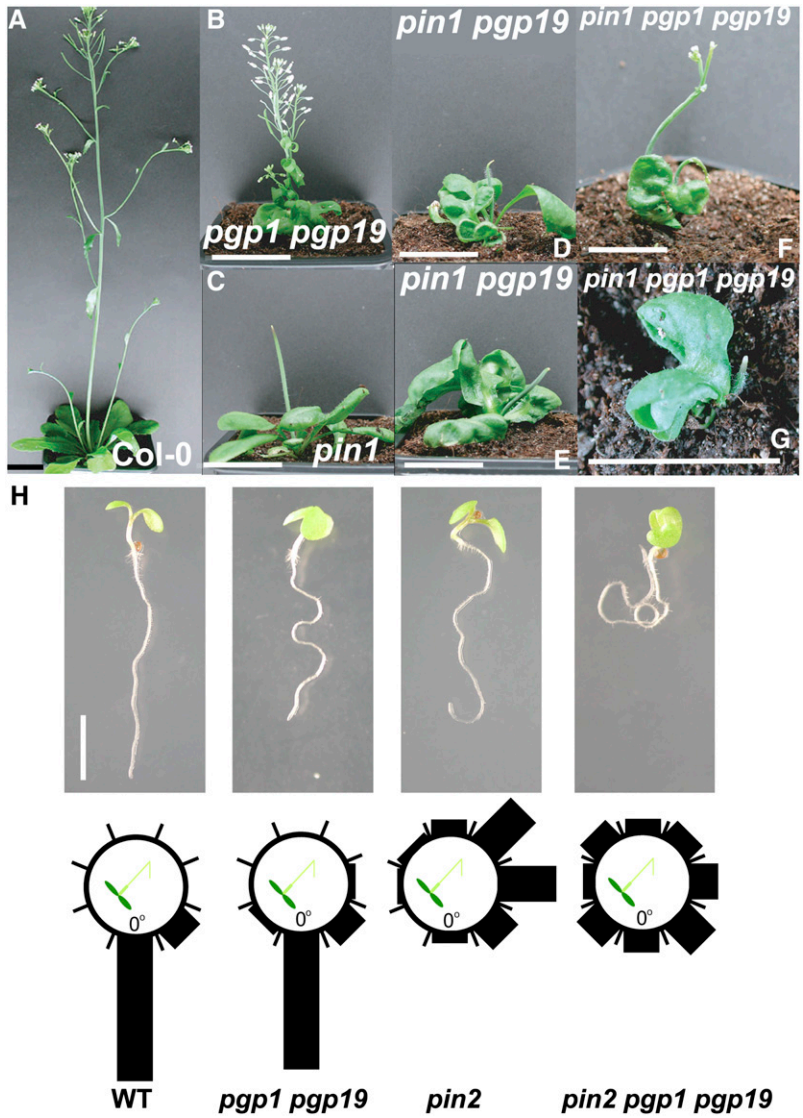

Figure 4. Phenotypes of *pgp pin* Mutants.

(A) Wild-type Columbia (Col-0) plant.
(B) *pgp1 pgp19* plant.
(C) *pin1* plant.
(D) *pin1 pgp19* plant
(E) Another *pin1 pgp19* plant.
(F) *pin1 pgp1 pgp19* plant.
(G) Another *pin1 pgp1 pgp19* plant.
(H) Root phenotypes of the wild type, *pgp1 pgp19*, *pin2*, and *pin2 pgp1 pgp19*. The number of roots in 30° sectors of a circle were counted and expressed as a percentage of the total number of roots. Vertical position represents normal gravitropic response. Values were calculated using 40 seedlings per experiment.
Bar = 5 cm in **(A)** to **(G)** and 1 cm in **(H)**.

mutants had a single pin-formed inflorescence stem, reduced secondary but no axillary inflorescences, wild type–like rosette, leaves, and no cauline leaves, flowers, or siliques (Figure 4C). The phenotypes of the single mutants were consistent with previously published reports (Okada et al., 1991; Gälweiler et al., 1998; Noh et al., 2001).

The *pin1 pgp19* double mutants had a single pin-formed inflorescence, no axillary or secondary inflorescences, and no flowers, siliques, or cauline leaves. They also had dwarf stature, reduced number of rosette leaves that were curlier than *pgp19* or *pgp1 pgp19* leaves, altered leaf margins, and occasionally more trichomes (Figures 4D and 4E). Reductions in leaf number were

also observed in *pin1 as1* mutants not observed in the single mutants, because ASYMMETRIC LEAVES1 (AS1) and PIN1 are functionally redundant in leaf initiation (Hay et al., 2006). The *pin1 pgp1 pgp19* triple mutants showed increased dwarf stature, loss of apical dominance, fused cotyledons, reduced number of rosette leaves, and curlier leaves with altered leaf margins (Figures 4F and 4G). Alterations in leaf margin phenotypes were observed in the double and triple mutants not observed in *pin1* or *pgp19* alone, consistent with leaf margin phenotypes in other mutants with perturbed local auxin gradients (Hay et al., 2006). Flowers develop in *pin1 pgp1 pgp19* plants, unlike in *pin1* or *pin1 pgp19* (Figure 4G), suggesting that the loss of *PGP1* is epistatic to *PIN1* in the shoot apex, as it partially restores floral development, presumably as a result of ectopic auxin accumulation in the shoot apical meristem. This partial floral rescue is similar to that in *pin1 bp* double mutants (Hay et al., 2006), suggesting that the altered local auxin accumulations in *pin1 pgp1 pgp19* may affect *BREVIPEDICELLUS* (*BP*) expression.

Crosses of *pin2* with *pgp* mutants were also made to determine whether there was a genetic interaction affecting root gravitropic phenotypes. Gravitropic bending is only slightly affected in *pgp19* (Geisler et al., 2005), *pgp1* has no detectable gravitropic phenotype (Noh et al., 2003), and *pin2* is agravitropic (Chen et al., 1998; Luschnig et al., 1998). In our hands, single *pin* and single or double *pgp* mutations exhibited only partial defects in gravitropic growth (Figure 4H). However, the *pin2 pgp1 pgp19* triple mutant exhibited completely agravitropic root growth (Figure 4H), similar to what is seen in *aux1* (Swarup et al., 2005). This finding suggests a synergistic interaction of PIN2 and PGPs in the root.

Loss of *PIN1* or *PGP19* Results in Decreased Transport Specificity in Planta

In whole plant auxin transport assays, BA is generally used as a control, because it is a weak organic anion that is poorly transported (Geisler et al., 2005). We had previously found that heterologous expression of PIN1, PIN2, PGP1, and PGP19 in nonplant systems activated increased levels of BA transport, suggesting that factors present in plants conferred additional auxin substrate specificity (Geisler et al., 2005; Bouchard et al., 2006; Petrášek et al., 2006). We reexamined basipetal BA transport in the wild type and *pin1*, *pgp1*, and *pgp19* mutants to ascertain whether the loss of one of these transport components resulted in increased BA transport. Basipetal BA transport in wild-type and *pgp1* seedlings was ~5% of IAA transport but was enhanced significantly in *pin1* and *pgp19* ($P < 0.05$; Figure 5). These results indicate that the absence of either PIN1 or PGP19 in planta reduces the substrate specificity of the transported anion, suggesting a biochemical interaction.

Biochemical Interaction Studies Suggest Specific PIN–PGP Interactions

Two independent methods were used to determine whether protein–protein interactions could occur between PGPs and PINs: coimmunoprecipitation and yeast two-hybrid assays. The identities of the proteins detected were confirmed by protein gel blotting and mass spectral analysis.

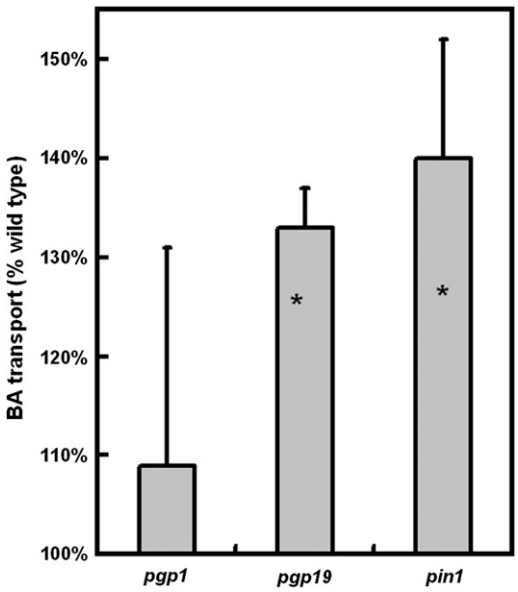

Figure 5. Substrate Specificity in Planta.

[^{3}H]BA transport in wild-type (Ws), *pgp1*, *pgp19*, and *pin1* seedlings. Data are means ± SD and are expressed as percentages of wild-type values ($n = 3$). * $P < 0.05$.

Coimmunoprecipitation Assays

Detergent-solubilized microsomal membrane proteins (microsomal proteins) from wild-type seedlings were incubated with polyclonal antiserum recognizing PGP1 and PGP19 (PGP1/19), fractionated by fast protein liquid chromatography, and analyzed by SDS-PAGE and protein gel blot analysis. Protein gel blot analysis using anti-PIN1 showed a signal at ~67 kD (Figure 6A), indicating that PIN1 coimmunoprecipitated with anti-PGP1/19. We repeated the assay with PGP19 antiserum and saw that PIN1 coimmunoprecipitated with PGP19 (Figure 6A). As a control, we repeated the assays using plasma membrane ATPase AHA2 antiserum, and PIN1 did not coimmunoprecipitate (Figure 6A). Additional controls included coimmunoprecipitations with PIN1, PGP19, and PGP1/19 antisera in the *pgp19*, *pgp1 pgp19*, and *pin1* mutant backgrounds; no signals were observed (see Supplemental Figure 2A online), indicating specificity of the antisera.

Microsomal proteins from Pro$_{35S}$:PGP19-HA transformants were incubated with PIN1 antiserum, and protein gel blots showed an ~136-kD signal with anti-HA, indicating that PGP19-HA coimmunoprecipitated with PIN1 (Figure 6B). Reciprocal coimmunoprecipitations of microsomal proteins from PGP19-HA overexpression lines were performed using anti-HA, and protein gel blots probed with PIN1 antiserum showed a signal at ~67 kD (see Supplemental Figure 2B online), supporting PIN1 and PGP19-HA coimmunoprecipitation. As a control, the supernatants and microsomal proteins from PGP19-HA and wild-type detergent-solubilized membranes were incubated with

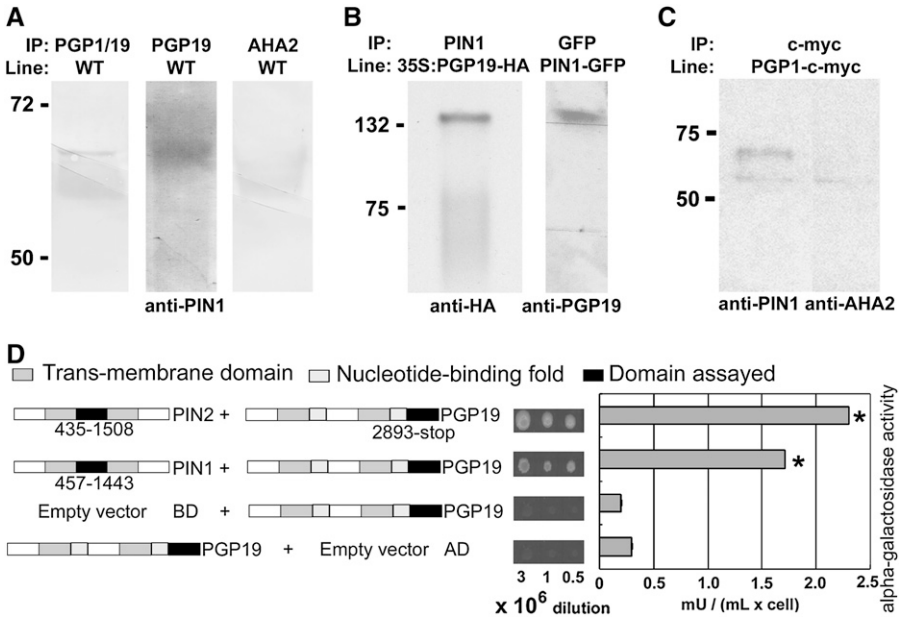

Figure 6. Protein–Protein Interactions Are Indicated in Coimmunoprecipitation and Yeast Two-Hybrid Assays.

(A) to **(C)** Coimmunoprecipitation assays.

(A) Detergent-solubilized proteins from 5-mg microsomal membranes from the wild type (Ws) immunoprecipitated (IP) with PGP1/19 antiserum (which strongly binds PGP1 but PGP19 less strongly; left), PGP19 antiserum (middle), or AHA2 antibody (right) as a control. The blots were probed with PIN1 antibody. PGP1/19, PGP19, and PIN1 coimmunoprecipitated. Samples were run on 12% gels.

(B) Detergent-solubilized proteins from 10-mg microsomal membranes from Pro_{35S}:PGP19-HA transformants coimmunoprecipitated with PIN1 antiserum (left). In the reciprocal experiment, PGP19 coimmunoprecipitated with PIN1-GFP in Pro_{PIN1}:PIN1-GFP transformants (right). Samples were run on 8% gels.

(C) Detergent-solubilized proteins from 10-mg microsomal membranes from Pro_{PGP1}:PGP1-cmyc transformants immunoprecipitated with cmyc antibody and probed with either PIN1 (left) or AHA2 (right) antiserum as a control. PGP1-cmyc coimmunoprecipitated PIN1 but not AHA2. A nonspecific band is observed on both blots. Coimmunoprecipitations are not quantitative. Samples were run on 8% gels.

(D) Yeast two-hybrid assays. Soluble loops of PIN1, PIN2, and the C terminus of PGP19 were used in yeast two-hybrid interaction assays and growth and α-galactosidase assays for MEL1 reporter gene expression. Empty binding domain (BD) or activation domain (AD) vectors were transformed with PGP19-AD vector or PGP19-BD vector, respectively, as negative controls. AD and BD constructs for reverse assays were also analyzed, and the results were the same as the data presented. In addition, the PIN-AD and PIN-BD assays showed no growth or α-galactosidase activity. Three transformants from 10 independent transformations for each pair of constructs were analyzed. Values shown are means $\pm$ SD ($n = 2$). * $P < 0.001$, as determined by Student's *t* test.

anti-HA, and no PIN1 signal was observed on the protein gel blots (see Supplemental Figure 2B online). As we were concerned that using PGP19-HA overexpression transformants for coimmunoprecipitation experiments might provide biased results, we repeated the experiments with Pro_{PIN1}:PIN1-GFP transformants. Microsomal proteins from Pro_{PIN1}:PIN1-GFP transformants were incubated with GFP antiserum, and the protein gel blots showed a signal with anti-PGP19 (Figure 6B). No signal was obtained when the experiments were repeated with wild-type microsomal proteins (see Supplemental Figure 2B online). This finding indicates that PIN1-GFP coimmunoprecipitated with PGP19.

Because the PGP1/19 antiserum reacts with both PGP1 and PGP19, we investigated PGP1 and PIN1 interactions. Microsomal proteins from Pro_{PGP1}:PGP1-cymc were incubated with cmyc antiserum. Protein gel blots probed with anti-PIN1 showed an ~67-kD signal (Figure 6C), indicating that PGP1-cmyc and PIN1 coimmunoprecipitated. As a control, protein gel blots were probed with AHA2, and no signal was observed (Figure 6C). Coimmunoprecipitation assays with PGP19, PGP1, and PIN2 were also conducted, and no signal was observed. Additionally, no signal was observed in coimmunoprecipitations with PGP4 and PIN1 or PIN2. These data suggest that PIN1 interacts with both PGP1 and PGP19.

Yeast Two-Hybrid Assays

The protein–protein interactive domains were mapped using yeast two-hybrid analyses. Yeast two-hybrid assays were performed with the C-terminal domain of PGP19, which has been shown to be a protein–protein interactive domain (Geisler et al., 2003), and the soluble loop regions of PIN1 and PIN2 (Figure 6D). PIN1 and PIN2 expression in yeast was confirmed by protein gel blots (see Supplemental Figure 2C online). When PIN1 and PIN2 were used as bait, an interaction with PGP19 was observed in both growth and α-galactosidase activity assays (Figure 6D). The

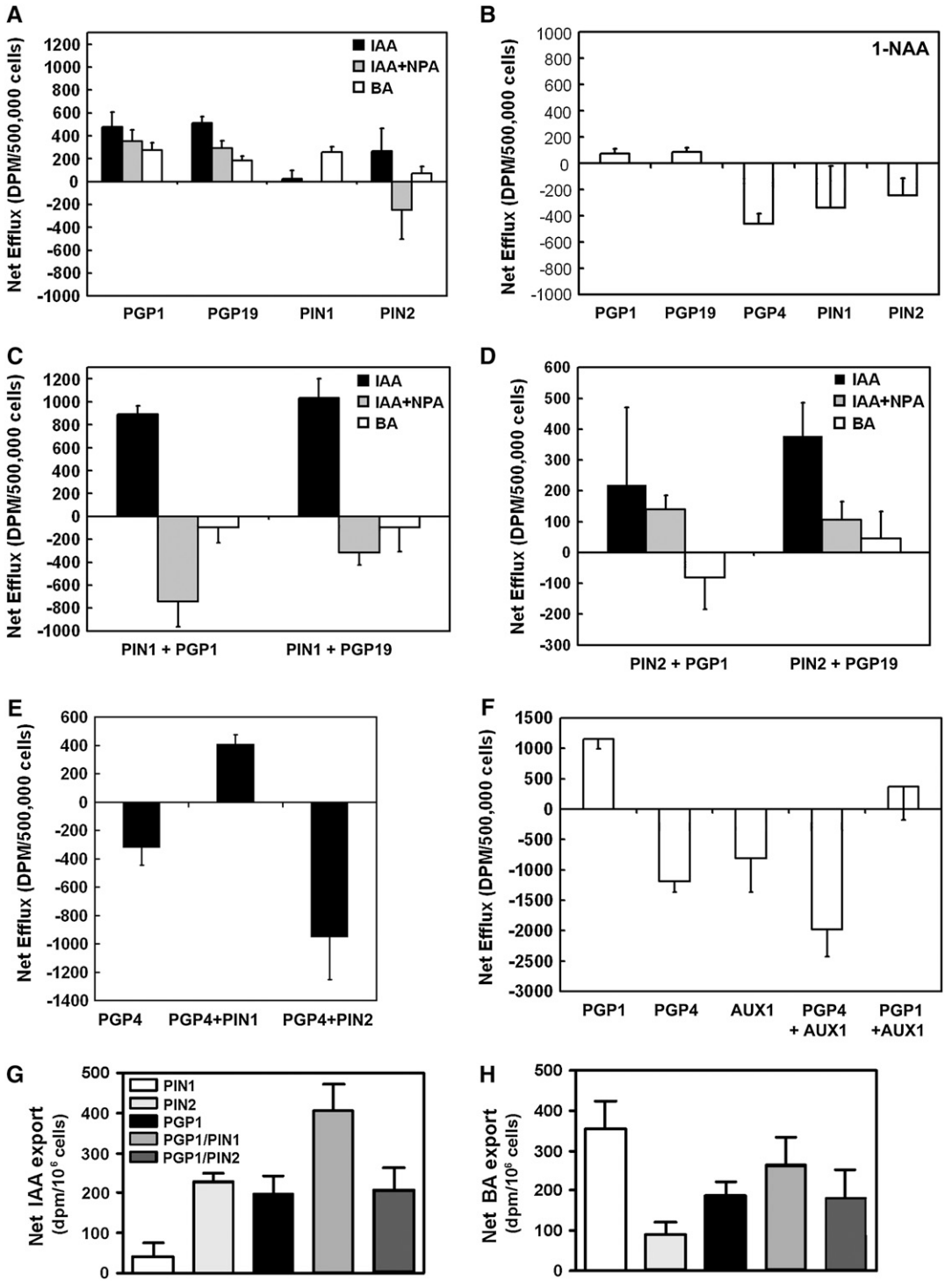

Figure 7. Coexpression of PIN and PGP Transporters Increases Substrate Specificity, Inhibitor Sensitivity, and Efflux.

(A) to **(F)** Efflux of radiolabeled substrates from HeLa cells expressing PGP1, PGP19, PIN1, or PIN2. Data are means with sum SD ($n = 3$).
(A) Net efflux of [^{3}H]IAA, [^{3}H]IAA in the presence of NPA, or [^{3}H]BA in HeLa cells expressing PGP1, PGP19, PIN1, PIN2, and AUX1. Baselines from a new set of experiments are presented only for the purpose of comparison with coexpression studies. Data for PGP1 and PIN2 were originally published by Geisler et al. (2005) and Petrášek et al. (2006). Efflux of substrates by PGP1 and PGP19 were significantly different from empty vector values ($P < 0.05$), and NPA inhibition of IAA efflux by PGP19 was significantly different compared with IAA alone ($P < 0.05$). BA efflux by PIN1 was significantly different from empty vector values ($P < 0.05$), as was IAA efflux by PIN2 ($P = 0.05$).

reverse assays using PGP19 as bait confirmed an interaction. Neither growth nor α-galactosidase activity was detected in negative controls using PGP19, PIN1, or PIN2 in the activation domain or the binding domain with empty vector in assays.

Interactions between full-length PGP19 and PIN1 could not be tested in the split-ubiquitin system because *PGP19* is not properly expressed in yeast as a result of hyperglycosylation (Noh et al., 2001; Geisler et al., 2005). In contrast with PGP19, no interactions were observed in yeast two-hybrid assays using the C-terminal region of PGP1 or PGP4 and the soluble loop of the PIN1 or PIN2 proteins. No interactions were observed in yeast two-hybrid assays using nucleotide binding fold 1 of PGP1, PGP4, or PGP19 with the soluble loop of PIN1 or PIN2. These results support the notion that PGP19 and PIN1 can interact and that PGP19–PIN interactions may be more specific than PGP1–PIN1 interactions (Noh et al., 2003).

Functional Interactions in Heterologous Systems

We investigated whether the observed protein–protein interactions had functional implications by coexpressing PGP and PIN proteins in the HeLa and yeast heterologous systems used previously to demonstrate transport activity (Geisler et al., 2005; Teresaka et al., 2005; Bouchard et al., 2006; Petrášek et al., 2006). Immunolocalizations confirmed that proteins expressed in HeLa cells were present on the plasma membrane (see Supplemental Figures 3A and 3B online), and fluorescence-activated cell sorting assays confirmed that cells expressing or coexpressing PGPs and PINs did not transport Hs MDR substrates (see Supplemental Figure 3C online). The substrate efflux profiles of PGP1, PGP19, PIN1, and PIN2 expressed in the HeLa system are presented in Figure 7A for reference. In the HeLa system PGP1, PGP19, and PIN2 mediated the efflux of the natural auxins IAA and BA, and IAA efflux was reduced in the presence of naphthylphthalamic acid (NPA) (Figure 7A). PIN1 did not mediate IAA efflux, but it did mediate BA efflux, like PGP1, PGP19, and PIN2 (Figure 7A). Substrate specificity was further analyzed using the synthetic auxin analog 1-naphthaleneacetic acid (1-NAA), and PGPs and PINs showed poor efflux of 1-NAA, indicating low affinity for 1-NAA compared with IAA (Figure 7B).

When PIN1 was coexpressed with PGP1 or PGP19 in HeLa cells, IAA efflux increased by ~1.8- or ~2-fold, respectively, compared with when the proteins were expressed alone (Figure 7C), indicating a synergistic interaction between PIN1 and PGP1 or PGP19. No IAA efflux occurred in the presence of NPA, and no BA efflux was observed (Figure 7C). Therefore, coexpression enhanced both inhibitor sensitivity and substrate specificity, supporting a functional interaction between PIN1 and PGP1 or PGP19.

By contrast, when PIN2 was coexpressed with PGP1 or PGP19 in HeLa cells, IAA efflux was reduced (27 and 47%, respectively) compared with the sum of the transport activities observed when each protein was expressed alone (Figure 7D). IAA efflux was inhibited in the presence of NPA, but the sensitivity to the inhibitor was not enhanced by coexpression. However, substrate specificity was still enhanced, as BA efflux was negligible (Figure 7D).

To further investigate whether the functional activity of PGP–PIN pairings was specific or nonspecific, we coexpressed PIN1 and PIN2 with PGP4. PGP4 localization does not coincide with PIN1 but does coincide with PIN2 localization in three cell stories in the central elongation zone (Müller et al., 1998; Steinmann et al., 1999; Terasaka et al., 2005). When PGP4 and PIN1 were coexpressed in HeLa cells, IAA efflux was observed (Figure 7E). This finding indicates that PIN1 interaction with PGP4 reversed PGP4 uptake transport activity. Coexpression of PGP4 and PIN2 enhanced auxin retention by approximately threefold compared with PGP4 expressed alone (Figure 7E). This suggests that a synergistic interaction between these proteins can occur, similar to that observed with PIN1 and PGP1 or PGP19. These data suggest that, in specific tissues in which PINs and PGPs colocalize subcellularly, specific interactions can occur; they also suggest that PIN proteins may regulate the directionality of PGP-mediated cellular transport across the plasma membrane in those tissues.

Figure 7. (continued).

(B) [^{3}H]1-NAA export by PGP1, PGP4, PGP19, PIN1, and PIN2. PIN1 specificity for 1-NAA was not different from IAA. PGPs and PIN2 had less affinity for 1-NAA than for IAA.

(C) Net efflux of [^{3}H]IAA, [^{3}H]IAA in the presence of NPA, or [^{3}H]BA in HeLa cells coexpressing PIN1 with PGP1 or PGP19. IAA efflux by PIN1+PGP1 or PGP19 was significantly different from that of each protein alone ($P < 0.05$). NPA inhibition of IAA efflux by PIN1+PGP1 or PGP19 was significantly different compared with IAA alone ($P < 0.05$). BA efflux was not different from empty vector values ($P > 0.05$).

(D) Net efflux of [^{3}H]IAA, [^{3}H]IAA in the presence of NPA, or [^{3}H]BA in HeLa cells coexpressing PIN2 with PGP1 or PGP19. IAA efflux by PIN2+PGP1 or PGP19 was significantly different from that of each protein alone ($P < 0.05$). NPA inhibition of IAA efflux by PIN2+PGP1 or PGP19 was significantly different compared with IAA alone ($P < 0.05$). BA efflux was not different from empty vector values ($P > 0.05$).

(E) Net efflux of [^{3}H]IAA in HeLa cells coexpressing PGP4 with PIN1 or PIN2. Coexpression of PGP4 with PIN1 reversed PGP4-mediated influx, resulting in auxin efflux. Coexpression of PGP4 with PIN2 led to a synergistic increase in auxin influx. IAA efflux by PGP4 was significantly different from that of empty vector alone ($P < 0.05$). IAA efflux by PGP4+PIN1 or PIN2 was significantly different compared with each protein alone ($P < 0.05$).

(F) Net efflux of [^{3}H]IAA in HeLa cells expressing AUX1, PGP1, or PGP4. AUX1 expressed in HeLa cells mediated IAA influx. When AUX1 was coexpressed with PGP4, an additive effect on net IAA influx was observed. When AUX1 was coexpressed with PGP1, net IAA transport was not observed.

(G) and **(H)** Efflux of radiolabeled IAA and BA from yeast cells expressing PGP1, PIN1, or PIN2. Data are means with SE ($n = 5$ for IAA and $n = 3$ for BA).

(G) Net [^{3}H]IAA export in yeast cells expressing PIN1, PIN2, or PGP1 or coexpressing PGP1 with PIN1 or PIN2. Coexpression of PGP1 with PIN1 synergistically increased auxin efflux, whereas coexpression of PGP1 with PIN2/AGR1/EIR1 led to decreased auxin efflux.

(H) Net [^{14}C]BA export in yeast cells expressing PIN1, PIN2, or PGP1 or coexpressing PGP1 with PIN1 or PIN2. Cells coexpressing PGP1 with PIN1 or PIN2 exhibited reduced BA efflux.

We also investigated whether the auxin influx carrier AUX1 could interact with PINs or PGPs. No interactions between AUX1–yellow fluorescent protein and PIN1 or PIN2 or PGP1, PGP4, or PGP19 were observed in coimmunoprecipitation assays, although occasionally a weak PIN1 signal was seen from coimmunoprecipitation with AUX1–yellow fluorescent protein from root tissues. Yeast two-hybrid assays of AUX1 (full-length AUX1 in the split-ubiquitin system, and C- and N-terminal domains of AUX1 in the GAL4 system) with soluble loops of PIN1 or PIN2 and C-terminal regions PGP1, PGP4, or PGP19 were inconclusive. AUX1-expressing HeLa cells mediated IAA influx (Figure 7F), consistent with previous results (Yang et al., 2006). When AUX1 was coexpressed with PGP4, an additive effect on net IAA influx was observed (approximately the sum of each expressed alone), but when it was coexpressed with PGP1, net IAA transport was not observed (Figure 7F). These data suggest that AUX1-mediated auxin transport does not involve direct PIN or PGP interactors.

When coexpression studies were recapitulated in the yeast *Saccharomyces cerevisiae* with greatly reduced background ABC transporter activity (Geisler et al., 2005; Petrášek et al., 2006), PIN1-mediated IAA export in yeast cells was negligible, whereas PIN2 and PGP1 had higher levels of IAA export (Figure 7G); protein gel blot analysis confirmed that PIN1 and PIN2 were expressed in yeast (see Supplemental Figure 3D online). Consistent with the net efflux observed in HeLa cells, coexpression of PGP1 and PIN1 synergistically increased IAA export in yeast cells (169% of the sum of each expressed alone), whereas coexpression of PGP1 and PIN2 was antagonistic (49% of the sum of each expressed alone) (Figure 7G).

As seen in HeLa cells, yeast cells expressing PIN1 alone exported more BA than PGP1 or PGP19, suggesting PIN1 activation of endogenous organic anion transporters or monocarboxylic acid transporters; PIN2 export of BA was low, as in HeLa cells (Figure 7H). Coexpression of PGP1 with PIN1 or PIN2 reduced BA export (49 and 66%, respectively, of the sum of each expressed alone), suggesting that coexpression imparted increased substrate specificity. PGP19 is not expressed properly in *S. cerevisiae* as a result of hyperglycosylation (Noh et al., 2001; Geisler et al., 2005).

Substrate specificity in HeLa cells was examined in competition and inhibition assays. In HeLa cells expressing PGP19 and PIN2, BA partially competed with IAA efflux (see Supplemental Figure 3E online). However, PGP19 mediated BA efflux to a greater extent than PIN2, suggesting that PIN2 has greater specificity for IAA than does PGP19. Another concern was that HeLa cells have background organic ion transporter (OAT) activity (Campbell et al., 2004; Wang et al., 2005) that might contribute to increased auxin efflux when PIN2, PGP1, or PGP19 is expressed in these cells (Geisler et al., 2005; Bouchard et al., 2006; Petrášek et al., 2006). In the empty vector, the OAT inhibitor cardio green resulted in a 14 $\pm$ 8.4% increase in IAA retention. Cardio green inhibited IAA efflux by $\sim$17% in PGP19 (similar to empty vector) and by $\sim$56% in PIN2 compared with the untreated respective controls (see Supplemental Figure 3E online). This finding indicates that PIN2 not only mediated IAA efflux but also activated an endogenous OAT activity in HeLa cells. As OAT orthologs are found in *Arabidopsis*, the impact of PIN activation of these transporters is unclear.

DISCUSSION

The results presented here support a model wherein PINs, PGPs, and AUX/LAX proteins define independent auxin transport mechanisms that function coordinately in planta. Although all PINs and PGPs (except PIN2) exhibit both polar and apolar subcellular localization, PINs are clearly the primary determinants of the directional auxin movement required for polar embryonic development, organ formation, and phyllotaxy. PGPs make a primary contribution to the export of auxin from apical tissues and play a major role in directing long-distance auxin transport in mature plants. Although PIN4 has been identified as a potential auxin sink in *Arabidopsis* roots (Friml et al., 2002a), all available data suggest that AUX/LAX proteins and, to a lesser extent, PGP uptake transporters such as PGP4 generate physiologically relevant auxin sinks required for the maintenance of auxin flow (Swarup et al., 2005; Terasaka et al., 2005). AUX1 appears to function independently, but specific PIN–PGP pairings influence polar auxin movement by enhancing substrate specificity and modulating rates of cellular auxin movement.

Analysis of expression, localization, and mutant phenotypes suggests that PINs and PGPs interact in planta. The absence of both PGP19 and PIN1 increased aberrant shoot morphology, and the absence of either decreased substrate specificity. Some PIN–PGP interactions, such as those between PIN1 and PGP19, appear to involve direct contacts between the proteins. However, localization studies suggest that such direct interactions are tissue-dependent. In subnodal light-grown hypocotyls, for instance, PGP19 localized in bundle sheath cells appears to function coordinately in redirecting auxin into the PIN1-mediated stream associated with vascular tissues, but it does not appear to contact PIN1 directly. Analyses of auxin movement in the wild type and *pin1*, *pgp1*, and *pgp19* suggests that PGP19 exclusion of auxin from cells surrounding the vascular cylinder enhances polar flow but also serves to export auxin to cortical tissues when auxin reaches a threshold level. The extent to which these functions contribute to the lateral redistribution of auxin in tropic bending (Noh et al., 2003) and lateral root formation is still not clear. It is also not yet determined whether interactions with PIN3 (Friml et al., 2002b) contribute to this PGP19-mediated activity.

However, in dark-grown and apical tissues, the subcellular coincidence of PIN1 and PGP19 is consistent with more direct interactions. As the coexpression of PINs and PGPs in heterologous systems results in enhanced inhibitor sensitivity, it is tempting to speculate that increased overlap of *PIN1* and *PGP19* expression in dark-grown *Arabidopsis* hypocotyls contributes to enhanced transport capability and the decreased growth inhibition by NPA (Jensen et al., 1998). However, as NPA inhibition of auxin transport in dark-grown hypocotyls has yet to be successfully assayed under nonphotomorphogenic conditions, a direct connection remains speculation.

Heterologous coexpression of PGP19 and PIN1 resulted in substrate specificity similar to that observed in whole plants and resulted in approximately twofold IAA transport compared with PGP19 alone. This finding suggests that where PIN1 and PGP19

colocalize, the rate of auxin transport can be greater than with either one alone. This synergistic effect may be enhanced by increased PIN1 stability on the plasma membrane observed in the presence of PGP19 (Noh et al., 2003). An increased rate of transport out of certain tissues has physiological relevance: PGP19 appears to function in auxin efflux out of the stele, and colocalization with PIN1 in the endodermis and pericycle would enhance this activity and serve as a component of an auxin reflux fountain model (Hasenstein and Evans, 1988; Wolverton et al., 2002; Swarup et al., 2004). Increased directional efflux within stelar tissues at the root tip would serve to enhance the polar auxin transport from the shoot apex and to increase the supply of auxin available for redirection within the lateral root cap (Swarup et al., 2005; Terasaka et al., 2005; Wisniewska et al., 2006).

Interactions between PGP1, PIN1, and PIN2 may be indirect, involve other domains of the proteins, or require partners other than PIN1 or PIN2, especially as the C-terminal regions of PGP1 and PGP19 interact with different protein domains of the immunophilin TWISTED DWARF1 (TWD1) (Geisler et al., 2003; Bouchard et al., 2006). PGP1 and PGP19 were also previously shown to interact with the glycosylphosphatidylinositol-anchored fascilin-like arabinogalactan protein FAGP2 (Murphy et al., 2002). However, yeast three-hybrid assays and coimmunoprecipitations with TWD1, FAGP2, PGP1, PGP19, PIN1, and PIN2 yielded either negative or inconclusive results. Coimmunoprecipitation and yeast two-hybrid results also suggest that other factors (protein, lipid, cytoskeleton, or cell wall) contribute to PGP–PIN interactions (Butler et al., 1998; Geisler et al., 2003; Pohl et al., 2005), and it is likely that PIN–PGP interactions are regulated by protein modification events such as phosphorylation (Friml et al., 2004; Nuhse et al., 2004).

As both PGP and PIN proteins have distinct localization patterns, and each protein is expected to contribute to a discrete, tissue-specific auxin transport stream, it will be necessary to develop a more complete map of PIN and PGP distribution within plant tissues. The *Arabidopsis PIN* gene family consists of 8 members and the *PGP* family consists of 21 members, all with overlapping expression patterns (Martinoia et al., 2002; Jasinski et al., 2003; Paponov et al., 2005). The evidence presented here and elsewhere (Noh et al., 2001; Peer et al., 2004; Geisler et al., 2005; Paciorek et al., 2005) also indicates that both *PGP* and *PIN* gene expression and consequent protein distribution are regulated by light and other factors. It is also likely that specific PGP–PIN interactions occur in cells in which both components are expressed and that other factors, such as TWD1, may regulate those interactions. Furthermore, the results presented here suggest that colocalization should not be the only criterion for positive interaction, as coexpression inhibited activity in some cases. Now that methods are in place to assay auxin transport activity (Geisler et al., 2005; Terasaka et al., 2005; Petrášek et al., 2006; Yang et al., 2006), every PIN and PGP must be assayed both individually and when coexpressed to determine the extent to which it contributes to auxin movement in planta. This information can be compared with the analysis of auxin transport and auxin-related growth phenotypes in mutants and used to construct a dynamic model of auxin transport that includes chemiosmotic and other regulatory factors (Li et al., 2005; Kramer, 2006).

METHODS

Real-Time Quantitative PCR

Real-time quantitative PCR was as described previously (Peer et al., 2004). *Arabidopsis thaliana* seedlings were grown as described by Murphy and Taiz (1995). Epidermal peels of upper inflorescence stems were prepared as described by Suh et al. (2005).

In Situ Hybridization

The method used was described by Grigg et al. (2005). PGP19 cDNA was cloned into pBluescript SK+, and sense and antisense PGP19 probes were prepared. Sections of 5-d-old dark- and light-grown seedlings were probed. Hybridization was visualized by digoxigenin labeling.

Immunolocalization

Pro_{PIN1}:PIN1-GFP (Benkova et al., 2003) seedlings were grown in the dark, and visualization was performed as described previously (Noh et al., 2003; Blakeslee et al., 2004), except that the seedlings were not fixed before imaging. Immunolocalizations in roots using the Triton X-100 series were performed according to the protocols of Peer et al. (2004). For PGP19 localization, the anti-PGP19 antibody was used at 1:800 dilution. Pro_{PIN1}:PIN1-GFP seedlings were used for coimmunolocalization of PIN1 and PGP19 according to the protocol described by Peer et al. (2004).

Whole mount immunolocalization was performed on 3- to 4-d-old seedlings grown vertically on Murashige and Skoog plates using the InsituPro roboter as described by Friml et al. (2003), except for using PBS instead of microtubule stabilizing buffer. The antibodies used were PIN1 (Gälweiler et al., 1998; Paciorek et al., 2005) at a final dilution of 1:1000, PIN2 (Müller et al., 1998) at a final dilution of 1:1000, HA.11 monoclonal antibody (BAbCO) at a final dilution of 1:800, and H^+-ATPase (Serrano et al., 1991) at a final dilution of 1:500. For the secondary antibodies, anti-rabbit fluorescein isothiocyanate and anti-mouse Cy3 (Dianova), the final dilution used was 1:600. Images were taken on Leica TSC and Zeiss LSM 210 META confocal microscopes.

PGP19 Antibody

Polyclonal anti-PGP19 antiserum was produced from a rabbit using 6× His–tagged PGP19 fragments containing amino acids 334 to 620. Anti-PGP19 antibodies were then purified form the antiserum using an antigen-blotted polyvinylidene difluoride membrane (Hybond-P; Amersham Biosciences). The amino acid sequence of antigen 334 to 620 is 5′-AGYKLMEIINQRPTIIQDPLDGKCLDQVHGNIEFKDVTFSYPSRPDVMIFRNFNIFFPSGKTVAVVGGSGSGKSTVVSLIERFYDPNSGQILLDGVEIKTLQLKFLREQIGLVNQEPALFATTILENILYGKPDATMVEVEAAASAANAHSFITLLPKGYDTQVGERGVQLSGGQKQRIAIARAMLKDPKILLLDEATSALDASSESIVQEALDRVMVGRTTVVVAHRLCTIRNVDSIAVIQQGQVVETGTHEELIAKSGAYASLIRFQEMVGTRDFSNPSTRRTRS-3′.

Pro_{PGP19}:PGP19-HA Construct

The genomic fragment of PGP19 (ATG to stop codon) was amplified by error-prone PCR and cloned to pGreenII-Kan (Hellens et al., 2000) through *Xho*I and *Xba*I sites. HA tag was introduced on the C terminus of the protein on the reverse primer. The 2-kb fragment of the PGP19 promoter was amplified by PCR and cloned to *Apa*I and *Sal*I sites. The 400-bp terminator region of PGP19 was amplified and cloned with *Bst*XI and *Not*I sites to create the final construct, pGreenPGP19-HA. The construct was transformed to Columbia wild-type plants by the standard floral-dip method (Clough and Bent, 1998). Transformants were selected on Murashige and Skoog medium plates with kanamycin (50 mg/L). The hypomorphic and epinastic phenotypes of *pgp19* were complemented by

transformation with Pro_{PGP19}:PGP19-HA, and these transformants were used to immunolocalize PGP19.

Coimmunoprecipitation Assays

Microsomal fractions were prepared from 2 to 3 g fresh weight of 21-d-old *Arabidopsis* plants and detergent-solubilized in ~1 mL of resuspension buffer using 0.1% Brij and 0.05% CHAPS, as described previously (Murphy et al., 2002). Solubilized proteins were incubated with anti-PGP1/19 for 2 h at 4°C. The anti-PGP1 antibody was originally raised against a fragment of PGP1 (Sidler et al., 1998) and had broad specificity for PGPs. However, after repurification, the antibody reacts with PGP1 and PGP19 (Geisler et al., 2003). The antibody also reacts with a 97-kD band (Geisler et al., 2003) subsequently determined by tryptic digest and mass spectrometry analysis to consist of truncated forms of PGP19 and PGP4. Antibodies were conjugated to ReactiGel or protein A–Sepharose (Pierce Biotechnology) according to the manufacturer's protocol before incubation. Anti-PGP19, anti-PGP4, anti-PIN1, anti-PIN2, anti-AHA2, anti-GFP, anti-HA, and anti-cmyc were also used. The slurry was transferred to a fast protein liquid chromatography column (Pharmacia), washed in 10 bed volumes of buffer A (10 mM BTP-MES, pH 7.8, 1 mM DTT, 0.1% Triton X-100, 1 mM phenylmethylsulfonyl fluoride, 200 ng/mL leupeptin, and 200 μM benzamidine), and eluted using a 20-min, 0.25 mL/min, 0 to 100% linear gradient of buffer B (1 M NaCl, 0.1 M Na-citrate, pH 3.0, 1 mM DTT, 0.1% Triton X-100, 1 mM phenylmethylsulfonyl fluoride, 200 ng/mL leupeptin, and 200 μM benzamidine). Fractions (0.5 mL) were precipitated with trichloroacetic acid, washed three times in acetone, resuspended in SDS buffer, and analyzed via 10% SDS-PAGE and protein gel blotting. The blot was probed with PIN1 antibodies from two different sources (Gälweiler et al., 1998; Paciorek et al., 2005), which yielded identical results.

Yeast Two-Hybrid Analysis

Constructs were designed to test the protein–protein interactions between PIN1 (At1g73590), PIN2 (At5g57090), and PGP19 (At3g28860). The PIN2 soluble region (453 to 1509 bp) and the PIN1 soluble region (457 to 1443 bp) were amplified by PCR. The following primers were used: PIN2 (EIR1-EcoRI-5, 5′-CGGAATTCCTCCGTGGGGCTAAGCTTCTCATC-3′; EIR1-PST1-3, 5′-GCTGCAGTGTTAGGGTTTCGAATGAGTTTT-3′); PIN1 (PIN1MID-5, 5′-CCGGAATTCGAGTACCGTGGAGCTAAG-3′; PIN1MID-3, 5′-CGTCTGCAGGGAGTAAGAGTTGGGATT-3′). PCR products were cloned into pGBKT7 via *Eco*RI and *Pst*I restriction sites to generate GAL4 DNA binding domain fusion proteins: MID-PIN2 and MID-PIN1. To generate GAL4 activation domain fusion partner proteins, the C terminus of PGP19 (2893 to stop) was amplified by PCR (MDR-C-5, 5′-CCGGAATTCGCAGCTCGAGCCGCAAAT-3′; MDR-PSTI-3, 5′-GCACTGCAGAATCCTATGTGTTTGAAG-3′). The PCR product was cloned into the pGAD424 vector (C-MDR1) as described above. Activation domain and binding domain constructs for reverse assays were also made as described above. Although some autoactivation of PGP19 was observed, the interaction of PGP19 with PINs was confirmed with reverse assays. All PCR-mediated cloned constructs were verified by sequencing. For interaction analysis, two combinatory constructs were transformed simultaneously into the AH109 yeast strain (Clontech) and tested for His3+, Trp+, Leu+, and Ade+ auxotrophy and MEL1 (α-galactosidase assay) reporter activity according to the manufacturer's protocols.

In Planta Transport Assays

Transport Assays in Inflorescences

Inflorescence auxin transport assays of *pin1-7* were as described by Noh et al. (2001).

Transport Assays in Whole 5-d-Old Seedlings

Transport assays in seedlings were as described by Geisler et al. (2003) with the exception that Whatman silica/cellulose paper was substituted as noted for assays of auxin export into the nonstelar apoplast. Briefly, ~100 nM IAA, applied as a 100-nL droplet of cold IAA (1 mM) in 20% DMSO, was placed on the root–shoot transition zone at the start of the transport assays. Nonstelar auxin movement was assayed by collection of discontinuous media strips supporting the mature root and counted in a scintillation counter to measure the diffusion of [^{3}H]IAA from cortical/epidermal apoplast.

HeLa Cell Transport Assays

For the radiolabeled substrate accumulation assay, PGP1 (At2g36910), PGP4 (At2g47000), PGP19 (At3g28860), PIN1 (At1g73590), PIN2 (At5g57090), and AUX1 (At5g01240) were expressed in mammalian HeLa cells using a vaccinia virus cotransfection system providing several advantages over other heterologous expression systems, including proper glycosylation and suppression of host protein synthesis after vaccinia infection (Elroy-Stein and Moss, 1990). The transient vaccinia expression system was used because stable cell lines develop mutations and express other endogenous drug-resistance mechanisms. Full-length PGP1, PGP19, PIN1, PIN2, and AUX1 cDNAs were cloned into the MCS of the pTM1 vector (Hrycyna et al., 1998). pTM1-PGP1, pTM1-PGP19, pTM-PGP4, and pTM-PIN2 were described previously (Geisler et al., 2005; Terasaka et al., 2005; Petrášek et al., 2006). For pTM1-PIN1, a *PIN1* PCR fragment containing *Nco*I/*Bam*HI restriction sites was generated using the following primers: PIN1-S, 5′-CATGCCATGGCAATGATTACGGCGGCGGAC-3′; PIN1-AS, 5′-CGCGGATCCAGCGTAATCTGGTACGTCGTATAGACCCAAGAGAATGTA-3′. For pTM1-AUX1, an *AUX1* fragment containing *Nco*I/*Bam*HI HA restriction sites was generated using the following primers: AUX1-S, 5′-CATGCCATGGGCATGTCGGAAGGAGTAGAA-3′; AUX1-AS, 5′-CGCGGATCCAGCGTAATCTGGTACGTCGTAAAGACGGTGGTGTAAAGC-3′. Assays for the accumulation of radiolabeled substrates were performed according to the method described by Geisler et al. (2005). Cells were transfected on six-well plates with 2 μg of DNA (pTM1 control vector, PGP1, PGP19, and PGP4) or 1.49 μg of DNA (PIN1 and PIN2) per well. The AUX1 amount transfected was 0.781 μg of DNA per well. For coexpression experiments, wells were transfected with 2 μg of PGP DNA and 1.49 μg of PIN DNA; the ratio of PGP to PIN DNA was empirically determined and found to be crucial for successful interaction.

For radiolabeled substrate accumulation assays, gradient conditions were developed wherein radiolabeled auxin was passively accumulated by empty vector control HeLa cells without induction of cellular damage. Confluent cells were transfected on six-well plates, and 16 to 24 h after transfection, cells were washed with 3 mL of prewarmed Dulbecco's modified Eagle's medium and 5% fetal bovine serum. Each transfection used 600,000 to 1,000,000 cells, and equal loading of wells was verified by sampled cell counts. Cells counts were determined by both Coulter counting and microscopic visualization (percentage confluence). Cells were then incubated with 2 mL of PBS citrate buffer, pH 5.5, and 5% calf serum containing either 10 or 62.5 nM of the following radiolabeled substrates: [^{3}H]IAA (specific activity, 26 Ci/mmol; Amersham Biosciences), [^{3}H]BA (specific activity, 20 Ci/mmol; American Rabiolabeled Chemicals), or [^{3}H]1-NAA (specific activity, 20 Ci/mmol; American Radiolabeled Chemicals). Possibly as a result of buffer compatibility issues, it was difficult to maintain the solubilization of 1-NAA in loading assays.

For radiolabeled auxin degradation product assays, cells were loaded with 10 nM radiolabeled IAA breakdown products (specific activity, 25 Ci/mmol; American Radiolabeled Chemicals). Cells were incubated with radiolabeled substrate for 40 min at 37°C and 5% CO_2. For inhibitor studies, cells were incubated with radiolabeled IAA in the presence of

10 μM NPA. After incubation, cells were washed three times each with 3 mL of ice-cold PBS, removed from the wells by trypsinization, and added to 18 mL of scintillation fluid. Samples were counted in a Perkin-Elmer scintillation counter. Components of the radiolabeled auxin breakdown product mixture were determined and quantified via liquid chromatography–mass spectrometry. Fluorescent substrate accumulation assays were performed in the HeLa cell system as described previously (Hrycyna et al., 1998). Data points were normalized to the average empty control vector value of 2851.885 dpm/500,000 cells for auxin treatments. Cell viability after treatment was confirmed visually and via cell counting. Net efflux is expressed as dpm/500,000 cells: the amount of auxin retained by cells transfected with empty vector minus the amount of auxin retained by cells transfected with the gene of interest. Reductions in auxin retention (efflux) in transfected cells are presented as positive values, whereas increases of auxin retention are presented as negative values. In all cases, expression and localization of expressed *Arabidopsis* proteins were confirmed by RT-PCR (Peer et al., 2004) and protein gel blotting (Hrycyna et al., 1998) using standard protocols for the system. Substrate integrity was determined by organic phase partitioning and mass spectral analysis.

Immunolocalization in HeLa Cells

HeLa cells were transfected as described above. Sixteen hours after transfection, cells were harvested with a rubber policeman, spun down, and fixed in methanol at room temperature for 10 min. Cells were permeabilized with 0.05% Triton X-100 for 5 min, washed, and incubated with anti-HA antibody (Roche Applied Science) or anti-PIN1 antibody (from J. Friml) at 37°C for 2 h. After primary antibody incubation, cells were washed and incubated with secondary antibody, anti-rabbit Alexa Fluor 546 (Molecular Probes) or anti-mouse fluorescein isothiocyanate (Miles-Yeda), for 45 min. Cells were washed, harvested, and imaged via confocal microscopy using argon and helium-neon lasers. Bright-field images were captured on a spot RT-CCD camera (Diagnostics).

Yeast Auxin Transport Assays

PIN1 (At1g73590) was amplified by RT-PCR from total root RNA as described by Geisler et al. (2005) using the following primers: PIN1-RT, 5′-ATAGACCCAAGAGAATGTAGTAG-3′; PIN1-S, 5′-ACGCTGCAGATGATTACGGCGGCGGACTTC-3′; and PIN1-AS, 5′-ACGGTCGACTCACGGCGCGCCTAGACCCAAGAGAATGTAGTA-3′. PIN1 was inserted with *Pst*I/*Sal*I into pAD4M (Luschnig et al., 1998), resulting in pAD4M-PIN1, and the absence of PCR errors was verified by sequencing. *Saccharomyces cerevisiae* strain JK93da containing pNEV-PGP1 or empty vector pNEV (Geisler et al., 2005) were transformed with pAD4M-PIN1, pADE1-HA (Luschnig et al., 1998), or empty vector pAD4M, and single colonies were grown in synthetic minimal medium without uracil and Leu, supplemented with 2% (w/v) glucose. Auxin efflux experiments were performed as described recently (Geisler et al., 2005) with the following modifications. Cells were loaded for 15 min on ice with combinations of 1 μL/mL [5-^{3}H]IAA (specific activity, 20 Ci/mmol; American Radiolabeled Chemicals) and [7-^{14}C]BA (53 mCi/mmol; Moravek Biochemicals). All aliquots were filtered on Whatman GF/C filters and washed three times with cold water, and retained radioactivity was quantified by scintillation counting. All transport experiments were performed three to five times with independent transformants, with four replicas each. Cell viability after treatment was confirmed visually. Auxin efflux was calculated by subtracting vector control values (dpm); net auxin efflux is expressed as dpm/10^{-6} cells.

Accession Numbers

Sequence data from this article can be found in the GenBank/EMBL data libraries under the following accession numbers: *PGP1* (At2g36910), *PGP4* (At2g47000), *PGP19* (At3g28860), *PIN1* (At1g73590), *PIN2* (At5g57090), and *AUX1* (At5g01240).

Supplemental Data

The following materials are available in the online version of this article.

Supplemental Figure 1. Summary of Auxin Transporter Localizations.

Supplemental Figure 2. Control Protein Gel Blot Analyses.

Supplemental Figure 3. Coimmunolocalization of PINs and PGPs on Plasma Membrane in HeLa cells, FACS Assays of HeLa Cells, Protein Gel Blot of PINs Expressed in Yeast, Cardio Green Inhibition of Auxin Transport, and BA Competition in HeLa Cells Expressing PIN2 or PGP19.

ACKNOWLEDGMENTS

We thank Ian Moore for sharing unpublished results and reagents to confirm protein localizations, for assistance in confocal laser scanning microscopy visualizations, and for helpful discussions of the manuscript. We thank Miltos Tsiantis and Angela Hay for their expertise and assistance with the in situ hybridizations. We thank David Smythe for the *pin1-7* seeds. We thank Petr Obrdlik for assistance with split-ubiquitin yeast two-hybrid assays. And we thank the reviewers for their advice on improving the manuscript. This work was supported by the U.S. National Science Foundation (Grant 0132803) and the Underwood Biotechnology and Biological Science Research Council (to A.S.M.); by the Volkswagenstiftung (to J.F., M.S., and J.M.); by the European Molecular Biology Organization Young Investigator Programme (to J.F.); by the Novartis Foundation and the Nissan Science Foundation (to T.S.); and by the Swiss National Science Foundation (to E.M.).

Received January 2, 2006; revised November 30, 2006; accepted December 7, 2006; published January 19, 2007.

REFERENCES

Ambudkar, S.V., Sauna, Z.E., Gottesman, M.M., and Szakacs, G. (2005). A novel way to spread drug resistance in tumor cells: Functional intercellular transfer of P-glycoprotein (ABCB1). Trends Pharmacol. Sci. **26:** 385–387.

Benkova, E., Michniewicz, M., Sauer, M., Teichmann, T., Seifertova, D., Jurgens, G., and Friml, J. (2003). Local, efflux-dependent auxin gradients as a common module for plant organ formation. Cell **115:** 591–602.

Bennett, M.J., Marchant, A., Green, H.G., May, S.T., Ward, S.P., Millner, P.A., Walker, A.R., Schulz, B., and Feldmann, K.A. (1996). *Arabidopsis AUX1* gene: A permease-like regulator of root gravitropism. Science **273:** 948–950.

Birnbaum, K., Shasha, D.E., Wang, J.Y., Jung, J.W., Lambert, G.M., Galbraith, D.W., and Benfey, P.N. (2003). A gene expression map of the *Arabidopsis* root. Science **302:** 1956–1960.

Blakeslee, J.J., Bandyopadhyay, A., Peer, W.A., Makam, S.N., and Murphy, A.S. (2004). Relocalization of the PIN1 auxin efflux facilitator plays a role in phototropic responses. Plant Physiol. **134:** 28–31.

Blakeslee, J.J., Peer, W.A., and Murphy, A.S. (2005). Auxin transport. Curr. Opin. Plant Biol. **8:** 494–500.

Blilou, I., Xu, J., Wildwater, M., Willemsen, V., Paponov, I., Friml, J., Heidstra, R., Aida, M., Palme, K., and Scheres, B. (2005). The PIN

auxin efflux facilitator network controls growth and patterning in *Arabidopsis* roots. Nature **433:** 39–44.

Bouchard, R., Bailly, A., Blakeslee, J.J., Oehring, S., Vincenzetti, V., Lee, O.R., Paponov, I., Palme, K., Mancuso, S., Murphy, A.S., Schulz, B., and Geisler, M. (2006). Immunophilin-like TWISTED DWARF1 modulates auxin efflux activities of *Arabidopsis* P-glycoproteins. J. Biol. Chem. **281:** 30603–30612.

Butler, J.H., Hu, S., Brady, S.R., Dixon, M.W., and Muday, G.K. (1998). In vitro and in vivo evidence for actin association of the naphthylphthalamic acid-binding protein from zucchini hypocotyls. Plant J. **13:** 291–301.

Callaghan, R., Ford, R.C., and Kerr, I.D. (2006). The translocation mechanism of P-glycoprotein. FEBS Lett. **580:** 1056–1063.

Campbell, S.D., de Morais, S.M., and Xu, J.J. (2004). Inhibition of human organic anion transporting polypeptide OATP 1B1 as a mechanism of drug-induced hyperbilirubinemia. Chem. Biol. Interact. **150:** 179–187.

Clough, S.J., and Bent, A.F. (1998). Floral dip: A simplified method for *Agrobacterium*-mediated transformation of *Arabidopsis thaliana*. Plant J. **16:** 735–743.

Chen, R.J., Hilson, P., Sedbrook, J., Rosen, E., Caspar, T., and Masson, P.H. (1998). The *Arabidopsis thaliana* AGRAVITROPIC 1 gene encodes a component of the polar-auxin-transport efflux carrier. Proc. Natl. Acad. Sci. USA **95:** 15112–15117.

Dawson, R.J., and Locher, K.P. (2006). Structure of a bacterial multidrug ABC transporter. Nature **443:** 156–167.

Elroy-Stein, O., and Moss, B. (1990). Cytoplasmic expression system based on constitutive synthesis of bacteriophage T7 RNA polymerase in mammalian cells. Proc. Natl. Acad. Sci. USA **87:** 6743–6747.

Friml, J., Benkova, E., Blilou, I., Wisniewska, J., Hamann, T., Ljung, K., Woody, S., Sandberg, G., Scheres, B., Jurgens, G., and Palme, K. (2002a). AtPIN4 mediates sink-driven auxin gradients and root patterning in *Arabidopsis*. Cell **108:** 661–673.

Friml, J., Benkova, E., Mayer, U., Palme, K., and Muster, G. (2003). Automated whole mount localisation techniques for plant seedlings. Plant J. **34:** 115–124.

Friml, J., Wisniewska, J., Benkova, E., Mendgen, K., and Palme, K. (2002b). Lateral relocation of auxin efflux regulator PIN3 mediates tropism in *Arabidopsis*. Nature **415:** 806–809.

Friml, J., et al. (2004). A PINOID-dependent binary switch in apical-basal PIN polar targeting directs auxin efflux. Science **306:** 862–865.

Gälweiler, L., Guan, C.H., Muller, A., Wisman, E., Mendgen, K., Yephremov, A., and Palme, K. (1998). Regulation of polar auxin transport by AtPIN1 in *Arabidopsis* vascular tissue. Science **282:** 2226–2230.

Geisler, M., et al. (2005). Cellular export of auxin by MDR-type ATP-binding cassette transporters of *Arabidopsis thaliana*. Plant J. **44:** 179–194.

Geisler, M., et al. (2003). TWISTED DWARF1, a unique plasma membrane-anchored immunophilin-like protein, interacts with *Arabidopsis* multidrug resistance-like transporters AtPGP1 and AtPGP19. Mol. Biol. Cell **14:** 4238–4249.

Geisler, M., and Murphy, A.S. (2006). The ABC of auxin transport: The role of P-glycoproteins in plant development. FEBS Lett. **580:** 1094–1102.

Goldsmith, M.H.M., and Goldsmith, T.H. (1977). Chemiosmotic model through plant tissue. Biophys. J. **17:** A260.

Grigg, S.P., Canales, C., Hay, A., and Tsiantis, M. (2005). SERRATE coordinates shoot meristem function and leaf axial patterning in *Arabidopsis*. Nature **437:** 1022–1026.

Hasenstein, K.H., and Evans, M.L. (1988). Effects of cations on hormone transport in primary roots of *Zea mays*. Plant Physiol. **86:** 890–894.

Hay, A., Barkoulas, M., and Tsiantis, M. (2006). ASYMMETRIC LEAVES1 and auxin activities converge to repress BREVIPEDICELLUS expression and promote leaf development in *Arabidopsis*. Development **133:** 3955–3961.

Heisler, M.G., Ohno, C., Das, P., Sieber, P., Reddy, G.V., Long, J.A., and Meyerowitz, E.M. (2005). Patterns of auxin transport and gene expression during primordium development revealed by live imaging of the *Arabidopsis* inflorescence meristem. Curr. Biol. **15:** 1899–1911.

Hellens, R.P., Edwards, E.A., Leyland, N.R., Bean, S., and Mullineaux, P.M. (2000). pGreen: A versatile and flexible binary Ti vector for Agrobacterium-mediated plant transformation. Plant Mol. Biol. **42:** 819–832.

Hrycyna, C.A., Ramachandra, M., Pastan, I., and Gottesman, M.M. (1998). Functional expression of human P-glycoprotein from plasmids using vaccinia virus-bacteriophage T7 RNA polymerase system. Methods Enzymol. **292:** 456–473.

Jasinski, M., Ducos, E., Martinoia, E., and Boutry, M. (2003). The ATP-binding cassette transporters: Structure, function, and gene family comparison between rice and Arabidopsis. Plant Physiol. **131:** 1169–1177.

Jensen, P.J., Hangarter, R.P., and Estelle, M. (1998). Auxin transport is required for hypocotyl elongation in light-grown but not dark-grown Arabidopsis. Plant Physiol. **116:** 455–462.

Kramer, E.M. (2006). How far can a molecule of weak acid travel in the apoplast or xylem? Plant Physiol. **14:** 1233–1236.

Li, J., et al. (2005). *Arabidopsis* H^+-PPase AVP1 regulates auxin-mediated organ development. Science **310:** 121–125.

Lin, R., and Wang, H. (2005). Two homologous ATP-binding cassette transporter proteins, AtMDR1 and AtPGP1, regulate Arabidopsis photomorphogenesis and root development by mediating polar auxin transport. Plant Physiol. **138:** 949–964.

Luschnig, C., Gaxiola, R.A., Grisafi, P., and Fink, G.R. (1998). EIR1, a root-specific protein involved in auxin transport, is required for gravitropism in *Arabidopsis thaliana*. Genes Dev. **12:** 2175–2187.

Marchant, A., Kargul, J., May, S.T., Muller, P., Delbarre, A., Perrot-Rechenmann, C., and Bennett, M.J. (1999). AUX1 regulates root gravitropism in *Arabidopsis* by facilitating auxin uptake within root apical tissues. EMBO J. **18:** 2066–2073.

Martinoia, E., Klein, M., Geisler, M., Bovet, L., Forestier, C., Kolukisaoglu, U., Muller-Rober, B., and Schultz, B. (2002). Multifunctionality of plant ABC transporters—More than just detoxifiers. Planta **214:** 345–355.

Müller, A., Guan, C.H., Galweiler, L., Tanzler, P., Huijser, P., Marchant, A., Parry, G., Bennett, M., Wisman, E., and Palme, K. (1998). AtPIN2 defines a locus of *Arabidopsis* for root gravitropism control. EMBO J. **17:** 6903–6911.

Multani, D.S., Briggs, S.P., Chamberlin, M.A., Blakeslee, J.J., Murphy, A.S., and Johal, G.S. (2003). Loss of an MDR transporter in compact stalks of maize br2 and sorghum dw3 mutants. Science **302:** 81–84.

Murphy, A., and Taiz, L. (1995). A new vertical mesh transfer technique for metal-tolerance studies in Arabidopsis. Ecotypic variation and copper-sensitive mutants. Plant Physiol. **108:** 29–38.

Murphy, A.S., Hoogner, K.R., Peer, W.A., and Taiz, L. (2002). Identification, purification, and molecular cloning of N-1-naphthylphthalmic acid-binding plasma membrane-associated aminopeptidases from Arabidopsis. Plant Physiol. **128:** 935–950.

Noh, B., Bandyopadhyay, A., Peer, W.A., Spalding, E.P., and Murphy, A.S. (2003). Enhanced gravi- and phototropism in plant mdr mutants mislocalizing the auxin efflux protein PIN1. Nature **423:** 999–1002.

Noh, B., Murphy, A.S., and Spalding, E.P. (2001). Multidrug resistance-like genes of *Arabidopsis* required for auxin transport and auxin-mediated development. Plant Cell **13:** 2441–2454.

Nourani, A., Wesolowski-Louvel, M., Delaveau, T., Jacq, C., and Delahodde, A. (1997). Multiple-drug-resistance phenomenon in the yeast *Saccharomyces cerevisiae*: Involvement of two hexose transporters. Mol. Cell. Biol. **17:** 5453–5460.

Nuhse, T.S., Stensballe, A., Jensen, O.N., and Peck, S.C. (2004). Phosphoproteomics of the *Arabidopsis* plasma membrane and a new phosphorylation site database. Plant Cell **16:** 2394–2405.

Okada, K., Ueda, J., Komaki, M.K., Bell, C.J., and Shimura, Y. (1991). Requirement of the auxin polar transport system in early stages of *Arabidopsis* floral bud formation. Plant Cell **3:** 677–684.

Paciorek, T., Zazimalova, E., Ruthardt, N., Petrášek, J., Stierhof, Y.D., Kleine-Vehn, J., Morris, D.A., Emans, N., Jurgens, G., Geldner, N., and Friml, J. (2005). Auxin inhibits endocytosis and promotes its own efflux from cells. Nature **435:** 1251–1256.

Paponov, I.A., Teale, W.D., Trebar, M., Blilou, I., and Palme, K. (2005). The PIN auxin efflux facilitators: Evolutionary and functional perspectives. Trends Plant Sci. **10:** 170–177.

Peer, W.A., Bandyopadhyay, A., Blakeslee, J.J., Makam, S.N., Chen, R., Mason, P., and Murphy, A. (2004). Variation in expression and protein localization of the PIN family of auxin efflux facilitator proteins in flavonoid mutants with altered auxin transport in *Arabidopsis thaliana*. Plant Cell **16:** 1898–1911.

Petrášek, J., et al. (2006). PIN proteins perform a rate-limiting function in cellular auxin efflux. Science **312:** 914–918.

Pohl, A., Devaux, P.F., and Herrmann, A. (2005). Function of prokaryotic and eukaryotic ABC proteins in lipid transport. Biochim. Biophys. Acta **1733:** 29–52.

Reinhardt, D., Pesce, E.R., Stieger, P., Mandel, T., Baltensperger, K., Bennett, M., Traas, J., Friml, J., and Kuhlemeier, C. (2003). Regulation of phyllotaxis by polar auxin transport. Nature **426:** 255–260.

Santelia, D., Vincenzetti, V., Azzarello, E., Bovet, L., Fukao, Y., Duchtig, P., Mancuso, S., Martinoia, E., and Geisler, M. (2005). MDR-like ABC transporter AtPGP4 is involved in auxin-mediated lateral root and root hair development. FEBS Lett. **579:** 5399–5406.

Serrano, R., Montesinos, C., Roldan, M., Garrido, G., Ferguson, C., Leonard, K., Monk, B.C., Perlin, D.S., and Weiler, E.W. (1991). Domains of yeast plasma membrane and ATPase-associated glycoprotein. Biochim. Biophys. Acta **1062:** 157–164.

Sidler, M., Hassa, P., Hasan, S., Ringli, C., and Dudler, R. (1998). Involvement of an ABC transporter in a developmental pathway regulating hypocotyl cell elongation in the light. Plant Cell **10:** 1623–1636.

Steinmann, T., Geldner, N., Grebe, M., Mangold, S., Jackson, C.L., Paris, S., Galweiler, L., Palme, K., and Jurgens, G. (1999). Coordinated polar localization of auxin efflux carrier PIN1 by GNOM ARF GEF. Science **286:** 316–318.

Suh, M.C., Samuels, A.L., Jetter, R., Kunst, L., Pollard, M., Ohlrogge, J., and Beisson, F. (2005). Cuticular lipid composition, surface structure, and gene expression in Arabidopsis stem epidermis. Plant Physiol. **139:** 1649–1665.

Swarup, R., et al. (2004). Structure-function analysis of the presumptive *Arabidopsis* auxin permease AUX1. Plant Cell **16:** 3069–3083.

Swarup, R., Kramer, E.M., Perry, P., Knox, K., Leyser, H.M., Haseloff, J., Beemster, G.T., Bhalerao, R., and Bennett, M.J. (2005). Root gravitropism requires lateral root cap and epidermal cells for transport and response to a mobile auxin signal. Nat. Cell Biol. **7:** 1057–1065.

Tanaka, H., Dhonukshe, P., Brewer, P.B., and Friml, J. (2006). Spatiotemporal asymmetric auxin distribution: A means to coordinate plant development. Cell Mol. Life Sci. **63:** 2738–2754.

Terasaka, K., Blakeslee, J.J., Titapiwatanakun, B., Peer, W.A., Bandyopadhyay, A., Makam, S.N., Lee, O.R., Richards, E.L., Murphy, A.S., Sato, F., and Yazaki, K. (2005). PGP4, an ATP binding cassette P-glycoprotein, catalyzes auxin transport in *Arabidopsis thaliana* roots. Plant Cell **17:** 2922–2939.

Wang, X., Wolkoff, A.W., and Morris, M.E. (2005). Flavonoids as a novel class of human organic anion-transporting polypeptide OATP1B1 (OATP-C) modulators. Drug Metab. Dispos. **33:** 1666–1672.

Weijers, D., Sauer, M., Meurette, O., Friml, J., Ljung, K., Sandberg, G., Hooykaas, P., and Offringa, R. (2005). Maintenance of embryonic auxin distribution for apical-basal patterning by PIN-FORMED-dependent auxin transport in *Arabidopsis*. Plant Cell **17:** 2517–2526.

Wisniewska, J., Xu, J., Seifertova, D., Brewer, P.B., Ruzicka, K., Blilou, I., Rouquie, D., Benkova, E., Scheres, B., and Friml, J. (2006). Polar PIN localization directs auxin flow in plants. Science **312:** 883.

Wolverton, C., Ishikawa, H., and Evans, M.L. (2002). The kinetics of root gravitropism: Dual motors and sensors. J. Plant Growth Regul. **21:** 102–112.

Yang, Y., Hammes, U.Z., Taylor, C.G., Schachtman, D.P., and Nielsen, E. (2006). High-affinity auxin transport by the AUX1 influx carrier protein. Curr. Biol. **16:** 1123–1127.

Yazaki, K., Shitan, N., Takamatsu, H., Ueda, K., and Sato, F. (2001). A novel *Coptis japonica* multidrug-resistant protein preferentially expressed in the alkaloid-accumulating rhizome. J. Exp. Bot. **52:** 877–889.

Yin, Y., He, X., Szewczyk, P., Nguyen, T., and Chang, G. (2006). Structure of the multidrug transporter EmrD from *Escherichia coli*. Science **312:** 741–744.